

Semiclassical and Continuum Limits of Four-Dimensional CDT

Jakub Gizbert-Studnicki

Abstract This Chapter discusses the infrared and the (perspective) ultraviolet limits of four-dimensional Causal Dynamical Triangulations (CDT). CDT is a non-perturbative and background-independent approach to quantization of Einstein's gravity, based on a lattice regularization of the quantum-gravitational path integral. It is shown that inside the, so-called, de Sitter phase one recovers a four-dimensional semiclassical universe, where behaviour of the scale factor is consistent with classical solutions of Einstein's field equations and fluctuations of the scale factor are very accurately described by a simple minisuperspace effective action. It is argued that some of the phase transitions bordering the semiclassical phase are higher-order transitions, which opens a possibility of defining a continuum limit of CDT. Finally, it is discussed how to define the renormalization group flow in CDT and then how to search for a UV fixed point in which, in the spirit of asymptotic safety, quantum theory of gravity could become non-perturbatively renormalizable and thus valid up to arbitrarily short distance scales.

Keywords

Lattice quantum gravity; Causal Dynamical Triangulations (CDT); Quantum geometry; Semiclassical limit; Phase transitions; Renormalization group (RG); Continuum limit; Asymptotic safety

Jakub Gizbert-Studnicki
Institute of Theoretical Physics, Jagiellonian University
ul. prof. S. Łojasiewicza 11, 30-348 Kraków, Poland
e-mail: jakub.gizbert-studnicki@uj.edu.pl

1 Introduction

Three out of four fundamental interactions are very accurately described by a quantum field theory (QFT), the infamous exception being the gravitational interaction. Therefore a quantum description of gravity remains an important goal of theoretical physics. Despite many different approaches described in this Handbook, yet to date there is still no fully consistent theory of quantum gravity. One of the problems one encounters when trying to apply QFT framework to quantization of General Relativity, which is currently our best description of the classical gravitational interaction, is that such an approach is perturbatively non-renormalizable. It means, that the naïve application of the perturbation theory would result in infinitely many counterterms and related coupling constants appearing in the theory in the ultraviolet (UV) limit, that cannot be eliminated via renormalization thus yielding the theory to be unpredictable. However, as suggested in Weinberg's seminal work [1], the definition of renormalizability might be generalised to the non-perturbative regime as described by the asymptotic safety conjecture. Asymptotic safety¹ predicts that the renormalization group (RG) flow of the bare gravitational couplings leads to the non-Gaussian UV fixed point(s), in which the quantum theory of gravity becomes scale-invariant (which by construction guarantees a constant limit, making the theory predictive), but also in the UV limit the dimensionless gravitational couplings do not need to be small (thus invalidating the naïve use of perturbation theory). The actual calculations using the functional renormalization group make approximations which can be difficult to control, and it is therefore important to verify the results by independent methods. This motivates a complementary lattice QFT approach which can potentially be used for testing the asymptotic safety scenario. In the lattice formulation the UV fixed point should appear as a higher-order critical point. The reason is the following: the divergent correlation length, characteristic for a higher-order phase transition, should allow taking the lattice spacing to zero while simultaneously keeping physical observables fixed; as the lattice spacing a plays a role of a UV regulator (providing the UV cutoff of the QFT of order $1/a$), the cutoff will be removed in the continuum limit, which hopefully should correspond to the UV fixed point of quantum gravity. At the same time, the lattice QFT in question should be able to correctly reconstruct the infrared (IR) limit of gravity, hopefully consistent with classical Einstein's field equations. In principle one should also be able to define how to renormalize the dimensionless bare lattice coupling constants when taking the lattice spacing to zero (or alternatively the UV cutoff to infinity). The RG flow of the couplings with decreasing lattice spacing should define some path(s) in the lattice coupling constant space leading from the IR semiclassical limit to the UV continuum limit.

¹ For more details check the part of the Handbook dedicated to the asymptotically safe quantum gravity and for the links of asymptotic safety with CDT refer to [2].

As will be argued below, one of the most successful lattice formulations of quantum gravity is that of Causal Dynamical Triangulations (CDT)², at least in the sense that it seems to admit a well defined semiclassical description and, at the same time, it has a rich phase structure, where some of the phase transitions might be higher-order transitions, and one can also define how to renormalize the bare couplings of CDT when the lattice spacing is changed; an open question remains if the flow of couplings really leads from the IR to the UV fixed point of quantum gravity. The approach is based on the lattice regularization of the quantum-gravitational path integral over metric d.o.f. (with Lorentzian signature)

$$Z_{QG}(G, \Lambda) = \int \mathcal{D}[g_{\mu\nu}] e^{iS_{EH}[G, \Lambda; g_{\mu\nu}]}, \quad (1)$$

where $\mathcal{D}[g_{\mu\nu}]$ is a measure term, which enables one to integrate over geometries, i.e., diffeomorphism-invariant equivalence classes of metrics $g_{\mu\nu}$, and S_{EH} is the Einstein-Hilbert action, dependent on the Newton's constant G and the cosmological constant Λ . In the four-dimensional CDT the continuous geometries are approximated by lattices (called *triangulations*) constructed from four-dimensional simplicial building blocks with fixed edge lengths (called *4-simplices*), fulfilling some additional topological constraints. The interior of each 4-simplex is isomorphic to a (part of) flat Minkowski spacetime and the geometry is encoded in the way the building blocks are "glued" together. This idea originates from earlier methods of Euclidean Dynamical Triangulations (EDT) [7], which assumed Euclidean (local $SO(4)$ symmetry) instead of Lorentzian (local $SO(3;1)$ symmetry) spacetime geometry. In EDT all simplices were equilateral and identical and the time direction was not distinguished. In contrast to that, in CDT one assumes that the (Lorentzian) spacetimes are globally hyperbolic and thus they admit a time-foliation into spatial hypersurfaces, called *slices*, of equal cosmological time. It is also required that the spatial topology Σ of each slice is fixed and preserved in the time evolution. As a result the spacetime topology is that of $[0, 1] \times \Sigma$. The (three-dimensional) geometry of a spatial slice at time t_k (k denotes the lattice time coordinate, $k \in \mathbb{Z}$) is represented by a triangulation $\mathcal{T}_k^{(3)}$ (with the fixed topology Σ) constructed from identical equilateral 3-simplices (tetrahedra). Any two such triangulations $\mathcal{T}_k^{(3)}$ at time t_k and $\mathcal{T}_{k+1}^{(3)}$ at time t_{k+1} constitute boundaries of a (four-dimensional) triangulation $\mathcal{T}_{k;k+1}^{(4)}$ of a *slab* between t_k and t_{k+1} , which can be constructed from four types of 4-simplices, denoted $T^{(4,1)}$, $T^{(1,4)}$, $T^{(3,2)}$ and $T^{(2,3)}$, where the numbers in parentheses represent the numbers of vertices that each simplex has in time t_k and t_{k+1} , respectively, see Fig. 1. The 4-simplices are "glued" together in such a way that there are no topological defects in the slab and thus any spatial hypersurface in time $t \in (t_k, t_{k+1})$ will also have the requested fixed topology Σ . The construction is repeated for $k = 1, 2, \dots, k_{max}$ to obtain a full four-dimensional triangulation \mathcal{T} with spatial boundaries $\mathcal{T}_1^{(3)}$ and $\mathcal{T}_{k_{max}}^{(3)}$. In practice, in order to avoid the necessity of

² For more details about the CDT formulation see [3] and review articles [4, 5, 6].

defining spatial boundary conditions, one usually identifies $\mathcal{T}_1^{(3)}$ and $\mathcal{T}_{k_{max}+1}^{(3)}$, i.e., one fixes the spacetime topology to be $S^1 \times \Sigma$ instead of $[0, 1] \times \Sigma$. The distinction of space and time introduced by the foliation is also present in the (fixed) edge lengths of the 4-simplices. This is quantified by the parameter α , defined by

$$a_t^2 = -\alpha a_s^2, \quad (2)$$

where a_t and a_s are the lattice spacing in the time and the spatial direction, respectively. According to Regge calculus [8], the curvature of a piece-wise flat simplicial manifold constructed from 4-simplices is defined through a deficit angle located at two-dimensional subsimplices (triangles) and depends on the number of 4-simplices sharing a given triangle. Using Regge prescription one can compute the Einstein-Hilbert action for a CDT triangulation \mathcal{T} , the so-called Regge action [3, 9]

$$S_R[k_0, k_4, \Delta; \mathcal{T}] = -(k_0 + 6\Delta)N_0 + k_4(N_4^{(4,1)} + N_4^{(3,2)}) + \Delta N_4^{(4,1)}. \quad (3)$$

The action is a linear combination of N_0 , denoting the total number of vertices, $N_4^{(4,1)}$, the total number of $T^{(4,1)}$ and $T^{(1,4)}$ 4-simplices, and $N_4^{(3,2)}$, the total number of $T^{(3,2)}$ and $T^{(2,3)}$ 4-simplices, in the triangulation \mathcal{T} . The three dimensionless bare coupling constants are k_0 , related to the inverse Newton's constant, k_4 , related to the cosmological constant, and Δ , related to the parameter α defined in equation (2).

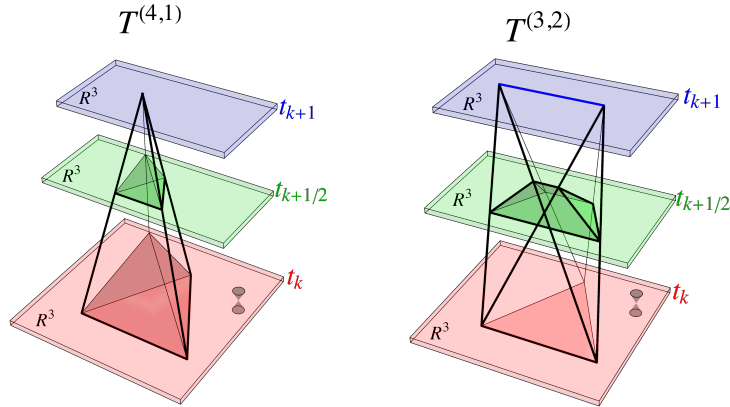


Fig. 1 The building blocks of the four-dimensional CDT triangulation: the $T^{(4,1)}$ simplex (left panel) and the $T^{(3,2)}$ simplex (right panel). The other two types, $T^{(1,4)}$ and $T^{(2,3)}$, are time-mirrored versions of them.

Using the CDT discretization the (formal) quantum-gravitational path integral (1) can be defined by

$$Z_{CDT}^{(L)}(k_0, k_4, \Delta, \Sigma) = \sum_{\mathcal{T} \in \mathcal{T}^{(L)}} \frac{1}{C_{\mathcal{T}}} e^{iS_R^{(L)}[k_0, k_4, \Delta; \mathcal{T}]}, \quad (4)$$

where the sum is over all possible CDT triangulations \mathcal{T} described above, the measure term $1/C_{\mathcal{T}}$ is the size of the automorphism group of \mathcal{T} and S_R is the Regge action (3), and we have used the index (L) to emphasize the Lorentzian setting. It is important to stress that despite the fact that in CDT one discretizes quantum geometries using triangulated manifolds with some finite lattice spacing a it is not assumed that the physical spacetime is discrete in any sense, and the UV cutoff $\sim 1/a$ (which regularizes the theory) is aimed to be removed in the continuum limit, if it exists. The four-dimensional CDT, defined by the lattice regularized path integral (4), cannot be solved analytically and in order to investigate its properties one is forced to use numerical methods which require a change from the Lorentzian to the Euclidean setting. Due to the introduced time-foliation the metric signature change is well defined. Wick rotation can be achieved by an analytic continuation $\alpha \rightarrow -\alpha$ ($\alpha > 7/12$) in the lower half of the complex α -plane. As a result the interior of each 4-simplex becomes isomorphic to a (part of) flat Euclidean space and the Regge action is changed accordingly such that $iS_R^{(L)} = -S_R^{(E)}$.³ The Euclidean Regge action $S_R^{(E)}$ is purely real and thus the CDT path integral (4) becomes a partition function

$$Z_{CDT}^{(E)}(k_0, k_4, \Delta, \Sigma) = \sum_{\mathcal{T} \in \mathcal{T}^{(E)}} \frac{1}{C_{\mathcal{T}}} e^{-S_R^{(E)}[k_0, k_4, \Delta; \mathcal{T}]}. \quad (5)$$

Note that the (Euclidean) triangulations \mathcal{T} appearing in the above sum must respect the imposed time-foliation and the fixed spatial topology Σ of the original (Lorentzian) triangulations, thus a memory of the Lorentzian setting is still kept.

The partition function (5) can be investigated using Monte Carlo (MC) methods. One performs MC simulations for a fixed topology Σ and a choice of points in the CDT bare coupling constants space (k_0, k_4, Δ) . The results of such simulations show that for fixed values of k_0 and Δ the partition function behaves in the leading order as

$$Z_{CDT}^{(E)}(k_0, k_4, \Delta, \Sigma) \propto e^{(k_4^c - k_4)N_4}, \quad (6)$$

where $N_4 = N_4^{(4,1)} + N_4^{(3,2)}$. The factor $e^{-k_4 N_4}$ comes directly from the bare cosmological constant k_4 appearing in the Regge action (3). The factor $e^{k_4^c N_4}$ comes from the number of states (triangulations with N_4 4-simplices) with the same value of the action, as the number of possible configurations grows (approximately) exponentially with N_4 , and the exponent k_4^c depends on k_0 and Δ . If $k_4 < k_4^c$ the partition function is divergent and the CDT theory becomes ill-defined. For $k_4 > k_4^c$ the size of the system remains finite. Therefore taking the infinite volume limit ($N_4 \rightarrow \infty$) requires

³ Both the Lorentzian $S_R^{(L)}$ and the Euclidean $S_R^{(E)}$ Regge actions have the same form as that of equation (3), just the functional dependence of the CDT bare coupling constants k_0, k_4, Δ on G, Λ, α must be appropriately adjusted.

at the same time fine-tuning $k_4 \rightarrow k_4^c$. In the MC simulations it is convenient to let the total lattice volume N_4 fluctuate around a fixed value \bar{N}_4 and perform a series of measurements for various target volumes \bar{N}_4 .⁴ For each \bar{N}_4 the k_4 coupling constant is fine-tuned to the pseudo-critical value $k_4 \rightarrow k_4^c(\bar{N}_4)$. In the limit $\bar{N}_4 \rightarrow \infty$ the finite-size effects vanish and one effectively obtains $k_4 \rightarrow k_4^c \equiv k_4^c(\infty)$. By fixing \bar{N}_4 one in fact studies the properties of $Z_{CDT}^{(E)}(k_0, \Delta, \bar{N}_4, \Sigma)$, which is linked with $Z_{CDT}^{(E)}(k_0, k_4, \Delta, \Sigma)$ by the Laplace transform

$$Z_{CDT}^{(E)}(k_0, k_4, \Delta, \Sigma) = \int_0^\infty d\bar{N}_4 e^{-k_4 \bar{N}_4} Z_{CDT}^{(E)}(k_0, \Delta, \bar{N}_4, \Sigma). \quad (7)$$

As a result, for the fixed topology Σ and the target lattice volume \bar{N}_4 , the partition function effectively depends only on two bare coupling constants k_0 and Δ . As will be shown below, at least in some region of the CDT parameter space, the dependence on \bar{N}_4 turns out to be universal and the \bar{N}_4 scaling analysis is a useful tool in discussing the semiclassical and the (perspective) continuum limits of CDT.

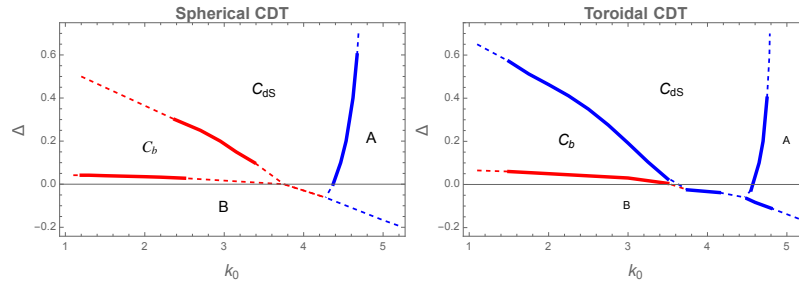


Fig. 2 The phase diagram(s) of the spherical (left panel) and the toroidal (right panel) CDT. Solid lines denote measured phase transition lines, where first-order transitions are shown in blue while higher-order transitions in red. Dashed lines are extrapolations.

The parameter space of the four-dimensional CDT spanned by k_0 and Δ has been largely investigated for the cases where the spatial topology Σ was chosen to be either S^3 (the, so-called, *spherical CDT*) or T^3 (the *toroidal CDT*). Four phases with distinct geometric properties have been found [10, 11, 12], see Fig. 2. Phase A is observed for sufficiently large values of the bare (inverse) cosmological constant k_0 . A typical configuration consists of many disjoint "baby universes" with a short time extension, see Fig. 3. In phase A the three-dimensional spatial volumes, quantified by the number of tetrahedra $N_3(k)$ forming a spatial slice with the lattice time coordinate $k \in \mathbb{Z}$, are uncorrelated. Phase B is realized for small values of the bare coupling Δ . In contrast to phase A, inside phase B the whole geometry "collapses" into a single spatial slice containing almost all spatial volume. The slice ends in the "past" and the "future" in a vertex of very high coordination number (belonging to almost all

⁴ In practice one usually fixes the $N_4^{(4,1)}$ volume.

4-simplices). The spatial volume outside the collapsed slice is close to the cutoff size, see Fig. 3. It is believed that these two phases can be understood essentially from the dynamics of the three-dimensional EDT geometries of the slices of constant (lattice) time. The spatial slices in phase A are presumably realizations of branched polymers which dominate the path integral of three-dimensional Euclidean quantum gravity for large k_0 , whereas the extended part of the geometry in phase B corresponds to the Euclidean geometry in the, so-called, crumpled phase, which is characterized by the presence of very few vertices with extremely high coordination number. The important feature of CDT, earlier unobserved in EDT is the existence of two new phases of quantum geometry. For sufficiently small values of κ_0 and positive, but not too-large Δ one can observe phase C_b . It shares some features with phase B , namely it contains vertices of very large coordination number, but, at the same time, it has a time-extended geometry, see Fig. 3. The presence of high-order vertices surrounded by volume clusters means that the geometry is quite inhomogeneous. Finally, for even higher values of the bare coupling Δ one reaches phase C_{dS} , whose generic geometry depends on the spatial topology choice, see Fig. 3. In the spherical CDT the geometry consists of the time-extended *blob*, where most three-volume is placed, and the spatial volume changes quite smoothly with the time coordinate, whereas in the toroidal CDT one observes a constant volume profile. The observed shape of the quantum universe closely resembles classical cosmological solutions of General Relativity. Therefore the phase C_{dS} can be considered to be related to the semiclassical limit of CDT.

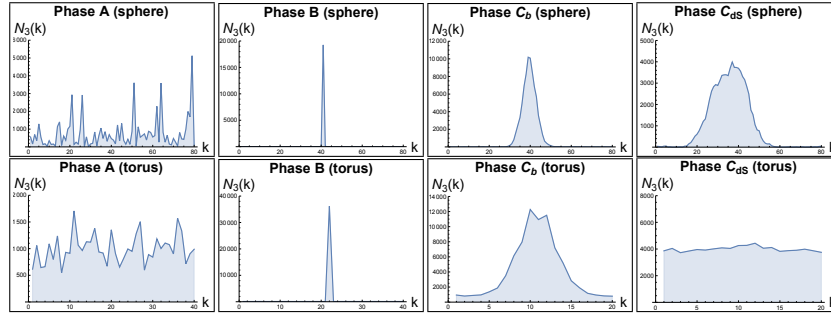


Fig. 3 Spatial volume profiles $N_3(k)$ of generic CDT configurations in different phases. Top: spherical CDT: A , B , C_b , C_{dS} ; Bottom: toroidal CDT: A , B , C_b , C_{dS} , respectively.

2 The semiclassical limit

As already mentioned in the introduction, in the four-dimensional CDT one obtains new phases of quantum geometry, earlier unobserved in EDT. The especially inter-

esting one is the phase C_{dS} , also called the *de Sitter* or the *semiclassical* phase. The hallmark of this phase is the presence of a stable extended four-dimensional geometry, where on large scales, compared to the triangulations size, a homogeneous and isotropic semiclassical spacetime with superimposed quantum fluctuations emerges dynamically. As will be discussed below, in phase C_{dS} not only does the effective macroscopic dimension of spacetime emerges with the correct classical value, but, equally remarkably, the global shape of the universe has been shown to be related to a simple minisuperspace description, similar to that used in standard quantum cosmology.

2.1 Evidence for the effective spacetime dimension four

It is important to stress that, in the path-integral formulation, the notion of spacetime dimension is an emergent concept. This is related to the fact that geometries entering the gravitational path-integral are not that of smooth four-dimensional manifolds and therefore the effective dimension can, and in general does, differ from the topological dimension. In the lattice regularized models, such as CDT, it exemplified by the fact that even though the 4-simplices forming triangulations are four-dimensional objects, due to the non-trivial connectivity structure, the triangulations cannot be embedded in the four-dimensional space. One should therefore define some notion of an effective dimension, which can be different (both larger or smaller) from the topological dimension.

2.1.1 The Hausdorff dimension

Due to the imposed time-foliation, one of the simplest observables⁵ measured in the Monte Carlo simulations of CDT is the so-called *spatial volume profile* $N_3(k)$. Each spatial slice with the lattice time coordinate $k \in \mathbb{Z}$ and the corresponding (continuous) time coordinate $t_k = k a$, where a is the lattice spacing⁶, is a three-dimensional triangulation constructed from identical equilateral tetrahedra. Accordingly, the continuum three-volume $V_3(t_k)$ is proportional to the number $N_3(k)$ of spatial tetrahedra in k

$$V_3(t_k) \propto a^3 N_3(k). \quad (8)$$

⁵ Here, by an *observable* we mean a quantity measured in the numerical simulations, not a diffeomorphism invariant observable.

⁶ In the following we will assume for simplicity that the effective lattice spacing a is the same in time and spatial directions. One can generalize to different lattice spacing a_t and a_s .

In the *spherical* CDT, the generic spatial volume profile observed in phase C_{dS} consists of an extended part, the so-called *blob*, whose ends are connected by a thin *stalk* where the spatial volume is of the minimal allowed cutoff size, see Fig. 3. During a MC simulation, due to the CDT time-translation symmetry, the blob performs a slow random walk around the (periodic) time-axis. Therefore, if one performed a long-enough MC simulation⁷ the spatial volume profile averaged over configurations would be a constant, in accordance with the time-translation symmetry. At the same time it is obvious that the presence of the blob means that individual CDT configurations in phase C_{dS} break the time-translation symmetry. One can take this into account when computing the average over configurations by appropriately shifting the center of volume of each individual MC generated configuration to a common time coordinate, say $k = 0$. As a result one gets a non-trivial one-point correlator, i.e., the *average volume profile* $\langle N_3(k) \rangle_{\tilde{N}_4}$, see Fig. 4, where the index \tilde{N}_4 denotes the constant target lattice volume fixed in a MC simulation.

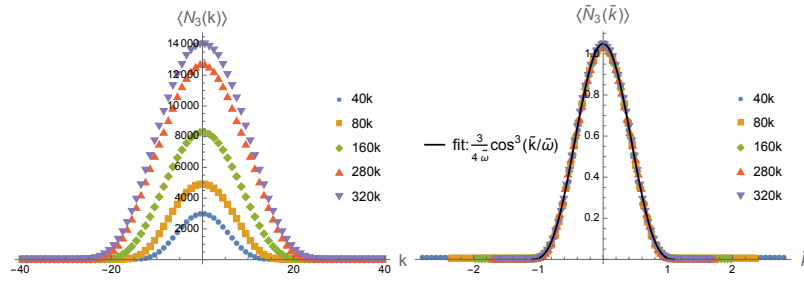


Fig. 4 Left panel: average volume profiles $\langle N_3(k) \rangle_{\tilde{N}_4}$ measured inside phase C_{dS} of the spherical CDT ($k_0 = 2.2$, $\Delta = 0.6$). Different colors denote different target lattice volumes $\tilde{N}_4^{(4,1)}$. Right panel: the volume profiles rescaled according to equation (9) with Hausdorff dimension $d_H = 4$ and the fit of equation (17).

If the effective spacetime dimension is d_H then, using textbook scaling arguments, one should expect that the spatially extended parts of the spacetimes measured for various effective four-volumes $\tilde{N}_4 = \langle \sum_{k \in \text{blob}} N_3(k) \rangle_{\tilde{N}_4}$, where the sum is over the extended part of the universe, can be mapped onto each other by rescaling the proper-time and the spatial volumes according to

$$k \rightarrow \tilde{k} = \frac{k}{\tilde{N}_4^{1/d_H}} \quad , \quad N_3(k) \rightarrow \tilde{N}_3(\tilde{k}) = \frac{N_3(k)}{\tilde{N}_4^{1-1/d_H}}. \quad (9)$$

As a result

$$\langle N_3(k) \rangle_{\tilde{N}_4} = \tilde{N}_4^{1-1/d_H} \langle \tilde{N}_3(\tilde{k}) \rangle = \tilde{N}_4^{1-1/d_H} H \left(\frac{k}{\tilde{N}_4^{1/d_H}} \right) \quad (10)$$

⁷ In practice such a simulation would take several years of computer time.

can be expressed in terms of a universal function H . The *Hausdorff dimension* d_H can be then measured by performing a series of MC measurements for systems of various size \tilde{N}_4 and fitting equation (10) by applying the best overlap method. In Fig. 4 we show that indeed, to a good approximation, our MC generated data measured in phase C_{dS} of the spherical CDT fit the above scaling relation with a classical value of Hausdorff dimension $d_H = 4$.

2.1.2 The spectral dimension

Another way of obtaining an effective dimension of spacetime appearing in a non-perturbative quantum gravity is to study a diffusion process of a fictitious point particle, related to the, so-called, *spectral dimension*, for more details see also [13].⁸ Let us consider a smooth d -dimensional Riemannian manifold \mathcal{M} equipped with a metric g_{ij} . The diffusion process is governed by the equation

$$\frac{\partial}{\partial \sigma} K(x, x_0; \sigma) = \Delta_g K(x, x_0; \sigma), \quad (11)$$

where σ is the fictitious diffusion time and Δ_g is the Laplace-Beltrami operator of the metric g_{ij} , with the initial condition peaked at $x_0 \in \mathcal{M}$, i.e., given by a delta function $K(x, x_0; \sigma = 0) = \delta^d(x - x_0)$. The heat kernel $K(x, x_0; \sigma)$ represents the probability density of finding a particle at position $x \in \mathcal{M}$ after a diffusion time σ . The average return probability to the origin after time σ

$$P_r(\sigma) = \frac{1}{V} \int dx \sqrt{g} K(x, x; \sigma), \quad (12)$$

where $V = \int dx \sqrt{g}$ is the volume of \mathcal{M} , has the following asymptotic expansion for small σ [15]

$$P_r(\tau) \sim \sigma^{-\frac{d}{2}} \sum_{i=0}^{\infty} A_i \sigma^i, \quad (13)$$

where A_i are generally complicated integrated functions of the metric g_{ij} . Note that the return probability (13) depends on the dimension d of the manifold. One can therefore compute the dimension from the return probability

$$d = -2 \lim_{\sigma \rightarrow 0} \frac{d \log P_r(\sigma)}{d \log \sigma}. \quad (14)$$

The expression (14) can be generalized by dropping the limit $\sigma \rightarrow 0$ which defines the (running) *spectral dimension*

⁸ The diffusion process discussed here is related to the *scalar* spectral dimension, one can also consider a more general diffusion of k -forms, see [14].

$$d_s(\sigma) = -2 \frac{d \log P_r(\sigma)}{d \log \sigma}. \quad (15)$$

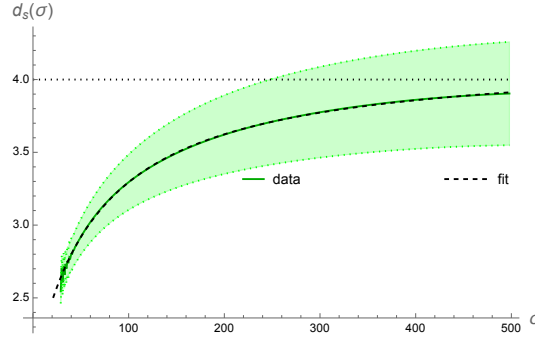


Fig. 5 The spectral dimension $d_s(\sigma)$ measured inside phase C_{dS} of the spherical CDT ($k_0 = 2.2$, $\Delta = 0.6$) and the fit of a phenomenological function (16). Shaded region indicates measurement errors.

In CDT one deals with discretized geometries and therefore one also has to discretize the diffusion equation (11). One typically considers the discrete diffusion on the *dual lattice*, i.e., the graph whose nodes are 4-simplices and whose links encode neighborhood relations between the 4-simplices. The diffusion process is originated at a randomly chosen 4-simplex of a given triangulation \mathcal{T} and the return probability is computed for a range of discrete diffusion steps $\sigma = 0, \dots, \sigma_{max}$. Then the (manifold) average return probability $P_r(\sigma)$ is estimated over a number of starting points $x_0 \in \mathcal{T}$. As we are interested in the expectation value of the above observable, the average $\langle P_r(\sigma) \rangle_{\tilde{N}_4}$ over the ensemble of triangulations is subsequently computed. Finally, the (expectation value of) spectral dimensions is calculated using equation (15). The results obtained in phase C_{dS} of the spherical CDT are presented in Fig. 5, where we also included a phenomenological fit

$$d_s(\sigma) = d + \frac{c}{\sigma + b}, \quad (16)$$

where the constants $d = 4.17 \pm 0.07$, $c = 146 \pm 28$, $b = 66 \pm 17$ were established from data in range $\sigma \in [30, 450]$. As can be seen the spectral dimension changes with the diffusion time σ , or otherwise with the geodesic distance, as the diffusion process probes larger and larger scales of the quantum geometry.⁹ The remarkable feature of the curve $d_s(\sigma)$ is its slow approach to the asymptotic value of $d_s(\sigma = \infty) = 4.17 \pm 0.07$ consistent with the four-dimensional universe. This type of behaviour is non-

⁹ One should note that for very large diffusion times σ , due to finite size effects, i.e., when the diffusion process probes the whole simplicial manifold (which is by construction closed in the chosen spacetime topology $S^1 \times S^3$), the zero modes of the Laplace-Beltrami operator dominate and the spectral dimension $d_s(\sigma)$ goes to zero. This part of the evolution is not shown on the plot and was not taken into account when fitting equation (16).

trivial and is not the case in other CDT phases. The other non-trivial phenomenon that has emerged dynamically is a scale dependence of the spectral dimension which goes to $d_s(\sigma = 0) \approx 2$ for short distances. It is related to non-classical features of generic geometries appearing in the CDT path integral. This non-trivial "dimensional reduction" has been first found in [16] and confirmed in many other approaches to quantum gravity [17, 18, 19, 20].

Summarizing this part, both the Hausdorff and the spectral dimensions measured in the C_{dS} phase point to the dynamically emerging macroscopic four-dimensional "average geometry". In the following we will provide evidence that indeed the geometry is consistent with a semiclassical four-dimensional universe.

2.2 Evidence for an effective minisuperspace action

2.2.1 The semiclassical de Sitter universe

In the lattice formulation one is interested in taking the thermodynamical (infinite volume) limit $\tilde{N}_4 \rightarrow \infty$, where one may hope to recover continuum physics. As already mentioned, inside phase C_{dS} of the spherical CDT the one-point correlator, i.e., the average spatial volume, shows a non-trivial scaling behaviour consistent with Hausdorff dimension four. One can therefore define a universal function $H(\tilde{k})$, describing the (rescaled) volume profile, see equation (10), which is independent of the lattice volume and thus it is also valid in the thermodynamical limit. A very nontrivial fact is that it is very well fitted by (cf. Fig. 4)

$$H(\tilde{k}) = \frac{3}{4\tilde{\omega}} \cos^3\left(\frac{\tilde{k}}{\tilde{\omega}}\right), \quad (17)$$

resulting in the universal scaling

$$\langle N_3(k) \rangle_{\tilde{N}_4} = \frac{3\tilde{N}_4}{4} \frac{1}{\tilde{\omega}\tilde{N}_4^{1/4}} \cos^3\left(\frac{k}{\tilde{\omega}\tilde{N}_4^{1/4}}\right). \quad (18)$$

The above is of course valid only inside the extended part of the universe (the blob), i.e., for $-\frac{\pi}{2}\tilde{\omega}\tilde{N}_4^{1/4} \leq k \leq \frac{\pi}{2}\tilde{\omega}\tilde{N}_4^{1/4}$. The constant $\tilde{\omega}$ appearing in equation (18) is a function on the CDT bare couplings k_0 and Δ . Restoring continuum quantities one can write

$$\begin{aligned}\langle V_3(t) \rangle &= \frac{3V_4}{4} \frac{1}{\omega V_4^{1/4}} \cos^3 \left(\frac{t}{\omega V_4^{1/4}} \right) = \\ &= 2\pi^2 \mathcal{R}^3 \cos^3 \left(\frac{t}{\mathcal{R}} \right),\end{aligned}\quad (19)$$

which is the volume profile of a regular four-sphere with physical volume V_4 and radius $\mathcal{R} = \omega V_4^{1/4}$, and where t is the (Euclidean) *proper-time*. It corresponds to the Wick rotated (Euclidean) de Sitter universe, i.e., a vacuum solution of Einstein's field equations with positive cosmological constant $\Lambda = 3/\mathcal{R}^2$. Such a solution is obtained for a maximally symmetric (spatially homogeneous and isotropic) metric with the infinitesimal line element squared

$$ds^2 = dt^2 + a^2(t) d\Omega_3^2, \quad (20)$$

where $a(t)$ is the scale factor and $d\Omega_3^2$ denotes the line element squared on the unit three-sphere, such that the spatial volume at proper-time t is $V_3(t) = 2\pi^2 a^3(t)$.

2.2.2 The effective action from volume fluctuations

So far we have looked only at the one-point function, i.e., the expected value of the spatial volume observable

$$\langle N_3(k) \rangle_{\tilde{N}_4} = \tilde{N}_4^{3/4} H \left(\frac{k}{\tilde{\omega} \tilde{N}_4^{1/4}} \right). \quad (21)$$

One can as well measure the two-point (connected) correlator

$$\langle \delta N_3(k) \delta N_3(k') \rangle_{\tilde{N}_4}, \quad (22)$$

where

$$\delta N_3(k) = N_3(k) - \langle N_3(k) \rangle_{\tilde{N}_4} \quad (23)$$

denote fluctuations around the dynamically emerging semiclassical average.

Let us first comment that the correlator (22) again shows the following universal scaling

$$\langle \delta N_3(k) \delta N_3(k') \rangle_{\tilde{N}_4} = \tilde{N}_4 F \left(\frac{k}{\tilde{\omega} \tilde{N}_4^{1/4}}, \frac{k'}{\tilde{\omega} \tilde{N}_4^{1/4}} \right) \quad (24)$$

with the same $\tilde{\omega}$, as in equation (21). The details of the function F are not important for the following discussion. Comparing equations (21) and (22) implies that the (relative amplitudes of) quantum fluctuations scale as

$$\frac{\sqrt{\langle \delta V_3^2(t_k) \rangle}}{\langle V_3(t_k) \rangle} = \frac{\sqrt{\langle \delta N_3^2(k) \rangle_{\bar{N}_4}}}{\langle N_3(k) \rangle_{\bar{N}_4}} \propto \frac{1}{\bar{N}_4^{1/4}}, \quad (25)$$

i.e., they vanish in the thermodynamical limit $\bar{N}_4 \rightarrow \infty$. As a result one obtains a fully classical spatial volume trajectory consistent with the de Sitter solution (19). Nevertheless, as will be shown below, analysis of quantum fluctuations described by the two-point correlator (24) is a useful tool to determine the *effective action* of CDT.

Let us consider a continuous model of quantum fluctuations around a well defined semiclassical trajectory $\bar{n}(t) \equiv \langle n(t) \rangle$. In a semiclassical approximation the quantum fluctuations $\delta n(t)$ around this trajectory are described by a Hermitian operator $P(t, t')$ obtained by a quadratic expansion of the effective action

$$S_{eff}[\bar{n}(t) + \delta n(t)] = S_{eff}[\bar{n}(t)] + \frac{1}{2} \int dt dt' \delta n(t) P(t, t') \delta n(t'), \quad (26)$$

where we neglect all terms of order $O(\delta n^3)$ in fluctuations. In a discretized model

$$S_{eff}[\bar{n}(t_k) + \delta n(t_k)] = S_{eff}[\bar{n}(t_k)] + \frac{1}{2} \sum_{kk'} \delta n(t_k) P_{kk'} \delta n(t_{k'}) \quad (27)$$

P becomes a matrix parametrized by a (discrete) time variable k

$$P_{kk'} = \left. \frac{\partial^2 S_{eff}}{\partial n(t_k) \partial n(t_{k'})} \right|_{n(t)=\bar{n}(t)}. \quad (28)$$

For such an expansion quantum fluctuations are Gaussian and the (discrete) two-point correlator, i.e., the covariance matrix, is given by the inverse of the propagator

$$C_{kk'} \equiv \langle \delta n(t_k) \delta n(t_{k'}) \rangle = \left(P^{-1} \right)_{kk'}. \quad (29)$$

The problem can simply be inverted. In numerical simulations one can measure the covariance matrix C . The inverse of the C matrix defines the (propagator) P matrix and thus the effective action S_{eff} , or at least its derivatives measured at the semiclassical solution (see equation (28)).

In order to apply the above method in the case of CDT, one should first check whether the quantum fluctuations are sufficiently well described by a quadratic effective action implying Gaussian fluctuations. This is indeed the case for the observed spatial volume fluctuations measured in the extended part of the CDT universe (the blob) in phase C_{dS} of the spherical CDT. Therefore the method seems applicable in the physically interesting limit of large lattice volumes. The empirical matrix \hat{P} , obtained by inverting the measured spatial volume-volume correlator \hat{C} has a simple tridiagonal structure, suggesting that there are only nearest neighbour interactions

between adjacent spatial slices. Consequently, the effective action can be expressed in the following form

$$S_{eff} = S_{kin} + S_{pot} = \sum_k K(N_3(k), N_3(k+1)) + \sum_k V(N_3(k)), \quad (30)$$

where the functions K and V , representing respectively the kinetic and the potential terms, have to be determined from empirical data. In order to do so let us make an Ansatz about a possible form of the effective action. As already mentioned, the semiclassical spatial volume profile is consistent with the de Sitter spacetime with spherical spatial topology, obtained for the metric (20). Inserting the metric to the (Euclidean) Einstein-Hilbert action

$$S_{HE}^{(E)} = -\frac{1}{16\pi G} \int dt \int d\Omega_3 \sqrt{g}(R - 2\Lambda) \quad (31)$$

one obtains the following *minisuperspace* action

$$S_{MS}^{(S^3)} = -\frac{3\pi}{4G} \int dt \left(a\dot{a}^2 + a - \frac{\Lambda}{3}a^3 \right). \quad (32)$$

The Euler-Lagrange equation of motion for the scale factor $a(t)$ derived from the action (32) is solved by

$$\bar{a}(t) = \mathcal{R} \cos\left(\frac{t}{\mathcal{R}}\right), \quad (33)$$

where we have chosen the proper-time to be in range $-\frac{\pi}{2}\mathcal{R} \leq t \leq \frac{\pi}{2}\mathcal{R}$, such that the maximum is located at $t = 0$. Reparametrizing $a(t)$ in terms of the spatial volume

$$V_3(t) = \int d\Omega_3 \sqrt{g|_{S^3}} = 2\pi^2 a^3(t) \quad (34)$$

one indeed obtains a solution consistent with the average CDT solution (19)

$$\begin{aligned} \bar{V}_3(t) &= 2\pi^2 \mathcal{R}^3 \cos^3\left(\frac{t}{\mathcal{R}}\right) = \\ &= \frac{3V_4}{4} \frac{1}{\omega V_4^{1/4}} \cos^3\left(\frac{t}{\omega V_4^{1/4}}\right), \quad V_4 = \int_{-\frac{\pi}{2}\mathcal{R}}^{\frac{\pi}{2}\mathcal{R}} dt \bar{V}_3(t). \end{aligned} \quad (35)$$

The constant $\omega = (\frac{3}{8\pi^2})^{1/4}$ is set by a condition that the total four-volume of the sphere is equal V_4 . The simplest discretization of the above continuum expression is given by

$$\bar{N}_3(k) = \frac{3\tilde{N}_4}{4} \frac{1}{\tilde{\omega}\tilde{N}_4^{1/4}} \cos^3\left(\frac{k}{\tilde{\omega}\tilde{N}_4^{1/4}}\right), \quad \tilde{N}_4 = \sum_k \bar{N}_3(k). \quad (36)$$

Comparing equations (35) and (36) one can identify

$$\frac{t_k}{\omega V_4^{1/4}} = \frac{k}{\tilde{\omega} \tilde{N}_4^{1/4}}, \quad V_4 = C_4 \tilde{N}_4 a^4, \quad (37)$$

where the (dimensionless) constant C_4 is the volume of a unit 4-simplex, a is the lattice spacing, and the continuum proper-time $t_k = k a$, implying

$$\tilde{\omega} = \omega C_4^{1/4}. \quad (38)$$

The minisuperspace action (32) can also be expressed in terms of the spatial volume (34)

$$S_{MS}^{(S^3)} = -\frac{1}{\Gamma} \int dt \left(\frac{\dot{V}_3^2}{V_3} + \mu V_3^{1/3} - \lambda V_3 \right), \quad (39)$$

where $\Gamma = 24\pi G$, $\mu = 9(2\pi^2)^{2/3}$ and $\lambda = 3\Lambda$. The simplest discretization of the above action has, up to a sign¹⁰, the following form

$$S_{eff}^{(S^3)} = \frac{1}{\tilde{\Gamma}} \sum_k \left(2 \frac{(N_3(k) - N_3(k+1))^2}{N_3(k) + N_3(k+1)} + \tilde{\mu} N_3(k)^{1/3} - \tilde{\lambda} N_3(k) \right), \quad (40)$$

which is the Ansatz we were looking for. The empirical propagator matrix \hat{P} , measured inside phase C_{dS} of the spherical CDT, is indeed very well described by the proposed Ansatz [21, 22]. The dimensionless coupling constants $\tilde{\Gamma}$, $\tilde{\mu}$ and $\tilde{\lambda}$ appearing in the discretized effective action (40) can be fitted from numerical data. Similarly to $\tilde{\omega}$ they all depend on the CDT bare couplings k_0 and Δ .

By analyzing relations between dimensionful and dimensionless quantities appearing respectively in the continuum expression (39) and its discrete counterpart (40) one obtains

$$\sqrt{C_4} a^2 \tilde{\Gamma} \tilde{\omega}^2 = \Gamma \omega^2, \quad (41)$$

$$\tilde{\mu} \tilde{\omega}^{8/3} = \mu \omega^{8/3}, \quad (42)$$

$$\tilde{\lambda} \tilde{\omega}^2 = \sqrt{C_4} a^2 \lambda \omega^2. \quad (43)$$

Rewriting (41) in terms of the Newton constant ($\Gamma = 24\pi G$; $\omega = (\frac{3}{8\pi^2})^{1/4}$) leads to

$$a^2 = \frac{6\sqrt{6}}{\sqrt{C_4} \tilde{\Gamma} \tilde{\omega}^2} G. \quad (44)$$

Assuming that the (renormalized) Newton Constant G is fixed and, as suggested by the CDT results, the semiclassical description is still valid close to the Planck length $\ell_p = \sqrt{G}$ (in units where $c = \hbar = 1$), one can use equation (44) to estimate

¹⁰ Note that the effective action of CDT agrees with the minisuperspace action up to an overall sign, see Conclusions for more discussion of this fact.

the effective lattice spacing (in $[\ell_p]$). The lattice spacing depends on two scales: the average size of the CDT universe expressed in lattice units (quantified by $\tilde{\omega}$) and the amplitude of quantum fluctuations (quantified by $\sqrt{\tilde{\Gamma}}$). The lattice spacing at the "generic" point in phase C_{dS} ($k_0 = 2.2, \Delta = 0.6$), where most of the CDT simulations were done, is estimated to be $a \approx 2 \ell_p$ which translates into an average radius of the MC generated quantum geometries $\sim 10 \ell_p$. It is remarkable that quantum universe at such short scales can be so well described by a semiclassical minisuperspace approximation.

2.2.3 The effective action from transfer matrix method

As argued above, the spatial volume distribution (or alternatively the scale factor) of the spherical CDT inside the S_{dS} phase is very well described by a simple discretization of the minisuperspace action (40). This result was obtained by analyzing a semiclassical approximation of volume fluctuations around the average (de Sitter) volume profile, where one could use the empirical covariance matrix to compute the propagator matrix. The problem with such an approach is that in a semiclassical approximation the propagator matrix is defined by second derivatives of the effective action at the semiclassical solution. One should note that the form of the discretized effective action (40) suggests that, in the physically interesting blob region, the second derivatives, i.e., the elements of the propagator matrix, fall very fast with increasing volume (derivatives of the kinetic term behave as $N_3(k)^{-1}$ and of the potential term as $N_3(k)^{-5/3}$). As a result it is very difficult to observe any subleading corrections, especially in the effective potential. A natural question arises if one can measure the effective action without resorting to the semiclassical approximation thus validating the above results.

The quasi-local form of a CDT discretized effective action (30) leads in a natural way to the path-integral representation of the spatial volume fluctuations

$$Z_{eff} = \sum_{\{N_3(k)\}} e^{-S_{eff}} \equiv \sum_{\{N_3(k)\}} \prod_{k=1, \dots, k_{max}} e^{-L_{eff}[N_3(k), N_3(k+1)]} = \text{tr} M^{k_{max}}, \quad (45)$$

where M is the *effective transfer matrix* defined by the effective Lagrangian

$$\langle N_3(k+1) | M | N_3(k) \rangle \propto \exp(-L_{eff}[N_3(k), N_3(k+1)]). \quad (46)$$

In the partition function (45) one assumes time-periodic boundary conditions, consistent with the CDT numerical setup. In such approach one disregards all details of the geometric structure at a given spatial slice and looks only at the spatial volume $N_3(k)$.

One should note that, by construction, CDT has a *genuine transfer matrix* \mathcal{M} which relates a spatial geometry $\mathcal{T}_k^{(3)}$ at the lattice time k to a spatial geometry $\mathcal{T}_{k+1}^{(3)}$ at time $k+1$. The transfer matrix \mathcal{M} is defined by a sum over all possible four-dimensional triangulations $\mathcal{T}_{k;k+1}^{(4)}$ of a slab between k and $k+1$ (with boundary three-dimensional triangulations $\mathcal{T}_k^{(3)}$ and $\mathcal{T}_{k+1}^{(3)}$)

$$\langle \mathcal{T}_{k+1}^{(3)} | \mathcal{M} | \mathcal{T}_k^{(3)} \rangle = \sum_{\mathcal{T}_{k;k+1}^{(4)}} e^{-S_R[\mathcal{T}_{k;k+1}^{(4)}]}, \quad (47)$$

where $S_R[\mathcal{T}_{k;k+1}^{(4)}]$ is the Regge action computed for the four-dimensional triangulation of the slab. Accordingly, the partition function of CDT (5) corresponding to k_{max} time steps (with time-periodic boundary conditions) can be expressed as

$$Z_{CDT} = \sum_{\{\mathcal{T}_k^{(3)}\}} \prod_{k=1, \dots, k_{max}} \langle \mathcal{T}_{k+1}^{(3)} | \mathcal{M} | \mathcal{T}_k^{(3)} \rangle = \text{tr} \mathcal{M}^{k_{max}}. \quad (48)$$

The effective transfer matrix elements can be formally computed as an average over the genuine transfer matrix elements

$$\langle N_3(k+1) | M | N_3(k) \rangle = \frac{1}{\mathcal{N}_{N_3(k+1)} \mathcal{N}_{N_3(k)}} \sum_{\substack{\mathcal{T}_{k+1}^{(3)} \in \mathcal{T}^{(3)}(N_3(k+1)) \\ \mathcal{T}_k^{(3)} \in \mathcal{T}^{(3)}(N_3(k))}} \langle \mathcal{T}_{k+1}^{(3)} | \mathcal{M} | \mathcal{T}_k^{(3)} \rangle, \quad (49)$$

where $\mathcal{T}^{(3)}(N_3(k))$ denotes a subset of all three-dimensional triangulations with size $N_3(k)$ and the number of such triangulations equals $\mathcal{N}_{N_3(k)}$. The statement that one can use the matrix M defined above as an effective transfer matrix assumes that the standard deviation of the matrix elements $\langle \mathcal{T}_{k+1}^{(3)} | \mathcal{M} | \mathcal{T}_k^{(3)} \rangle$ in equation (49) is sufficiently small and consequently

$$\langle \mathcal{T}_{k+\Delta k}^{(3)} | \mathcal{M}^{\Delta k} | \mathcal{T}_k^{(3)} \rangle \sim \langle N_3(k+\Delta k) | M^{\Delta k} | N_3(k) \rangle, \quad (50)$$

for $\Delta k = 1, 2, \dots, k_{max}$. In the following we will assume that the description of spatial volume fluctuations using the effective transfer matrix M is a sufficiently good approximation and use it to analyze the empirical (Monte Carlo generated) data. The consistency of such analysis will provide indirect evidence that the approach is correct.

Using the partition function (45) and the resulting effective transfer matrix M one can compute the (two-point) probability distribution of measuring a combination of volumes $N_3(k) = n$, $N_3(k') = m$ ($n, m \in \mathbb{N}$) in spatial slices separated by $\Delta k = k' - k$ time steps

$$P_{\Delta k}^{k_{max}}(N_3(k) = n, N_3(k') = m) = \frac{1}{Z_{eff}} \langle n | M^{k_{max}-\Delta k} | m \rangle \langle m | M^{\Delta k} | n \rangle, \quad (51)$$

where we again assumed time-periodic boundary conditions. Let us consider a CDT model with a very short time period $k_{max} = 2$. It follows from equation (51) that the two-point probability distribution of measuring $N_3(1) = n$ and $N_3(2) = m$ is given by

$$P_{\Delta k=1}^{k_{max}=2}(N_3(1) = n, N_3(2) = m) = \frac{\langle n|M|m\rangle\langle m|M|n\rangle}{\text{tr}M^2}. \quad (52)$$

Due to time reflection symmetry the transfer matrix M must be symmetric, leading to

$$\langle n|M|m\rangle = \mathcal{N}_0 \sqrt{P_{\Delta k=1}^{k_{max}=2}(N_3(1) = n, N_3(2) = m)}. \quad (53)$$

The empirical two-point probability distribution $\hat{P}_{\Delta k=1}^{k_{max}=2}$ can be measured in the MC simulations of CDT and therefore used to estimate the transfer matrix elements (up to a normalization factor \mathcal{N}_0), see Fig. 6, where we show (the logarithm) of the transfer matrix elements measured in phase C_{dS} of the spherical CDT. The empirical transfer matrix can be then used to reconstruct the effective Lagrangian L_{eff} . According to equation (46) one gets

$$L_{eff}[n, m] = -\log\langle n|M_{eff}|m\rangle + \log\mathcal{N}_0 \quad (54)$$

and the corresponding effective action is given by

$$S_{eff} = \sum_k L_{eff}[N_3(k), N_3(k+1)]. \quad (55)$$

For very small spatial volumes ($N_3 < \sim 300$) the effective Lagrangian is dominated by lattice discretization artifacts (Fig. 6, left), but for larger volumes it is quite smooth (Fig. 6, right) and can be very well fitted by the following (discretized) Lagrangian [23]

$$L_{eff}^{(S^3)}[n, m] = \frac{1}{\tilde{\Gamma}} \left[2 \frac{(n-m)^2}{n+m-2n_0} + \tilde{\mu} \left(\frac{n+m}{2} \right)^{1/3} - \tilde{\lambda} \left(\frac{n+m}{2} \right) \right], \quad (56)$$

where we have omitted a constant term $\log\mathcal{N}_0$. Fitted values of the parameters $\tilde{\Gamma}$, $\tilde{\mu}$ and $\tilde{\lambda}$ agree within measurement errors with the parameters obtained using the covariance matrix method discussed above. In the above discretization we have also included a (very small¹¹) finite-size correction n_0 . Note that in (56) we have also used a different discretization of the potential part of the effective Lagrangian than in equation (40). Such a form better fits the transfer matrix data but it gives exactly the same continuum effective action, consistent with the minisuperspace action (39).

In order to check the validity of the effective transfer matrix approach one can compare the spatial volume fluctuations data measured in CDT and in a simplified effective model, defined by the partition function (45), where the spatial volume is the only degree of freedom. The transfer matrix M used in the effective model is obtained by smoothly joining the purely empirical transfer matrix \hat{M} , measured for

¹¹ Fitted values of $|n_0| < 10$ are very small compared to macroscopic spatial volumes $N_3 > 300$, where discretization effects are negligible and the parametrization (56) holds.

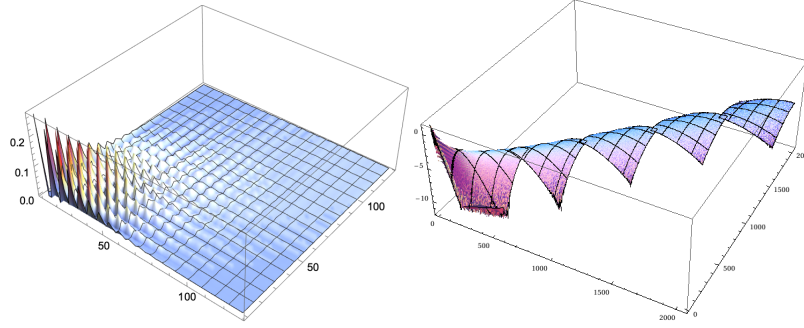


Fig. 6 Empirical transfer matrix measured for small (left panel) and large (right panel) spatial volumes in phase C_{dS} of the spherical CDT ($k_0 = 2.2, \Delta = 0.6$). Right figure is in logarithmic scale.

very small spatial volumes where discretization artifacts prevail, with the theoretical transfer matrix $M_{th}^{(S^3)} \equiv \mathcal{N}_0 \exp(-L_{eff}^{(S^3)})$ defined by the effective Lagrangian (56) (with fitted values of $\tilde{\Gamma}, \tilde{\mu}$ and $\tilde{\lambda}$), applicable to larger volumes, i.e.,

$$\langle n|M|m \rangle = \begin{cases} \langle n|\hat{M}|m \rangle & , n < thr \text{ or } m < thr \\ \langle n|M_{th}^{(S^3)}|m \rangle & , \text{ otherwise} \end{cases}, \quad (57)$$

where thr is a threshold ($thr = 300$). In Fig. 7 we compare the average spatial volume profile and the fluctuations profile measured in both the effective and the original CDT Monte Carlo simulations [24]. The agreement is indeed remarkable thus validating the form of the effective action.

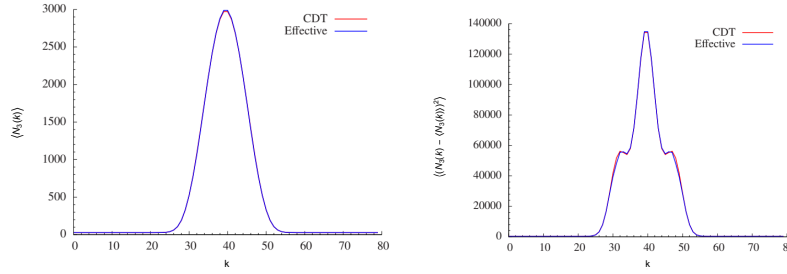


Fig. 7 Comparison of the full CDT results with the effective model of spatial volume fluctuations described in the text. Left panel shows the average volume profile $\langle N_3(k) \rangle$ and right panel the fluctuations profile $\langle (N_3(k) - \langle N_3(k) \rangle)^2 \rangle$. Data measured in phase C_{dS} of the spherical CDT ($k_0 = 2.2, \Delta = 0.6$).

2.2.4 Impact of the spatial topology choice

All the results discussed above were obtained in the CDT model with a (fixed) spherical spatial topology $\Sigma = S^3$. As discussed in the introduction, the spatial topology choice is an important ingredient of CDT, it is therefore important to check the impact of the topology choice on the results. So far, the only other spatial topology studied in the MC simulations was the toroidal topology $\Sigma = T^3 \equiv S^1 \times S^1 \times S^1$, and such a topology change (from spherical to toroidal) does not seem have impact on the CDT phase structure, see Fig. 2. All four phases (A , B , C_b and C_{dS}) earlier observed in the spherical CDT are also present in the toroidal CDT. Also location of all phase transition lines is similar for both topologies.¹² Nevertheless, due to the different spatial topologies the dynamically emerging background geometry observed in phase C_{dS} can be different. It is indeed the case as can be visualized by the spatial volume profiles measured in phase C_{dS} , see Fig. 3. In the spherical CDT the average volume profile was very well fitted by a \cos^3 function, cf. equation (18), while in the toroidal CDT one rather observes a constant volume profile $\langle N_3(k) \rangle_{\bar{N}_4} = \text{const}$.

As discussed above, in the spherical CDT the spatial volume fluctuations are very accurately explained by the minisuperspace effective action, see equation (39), where the potential term $\propto V_3(t)^{1/3}$ comes from a (constant positive) curvature of the three-sphere and therefore is absent in the case of the (flat) topological torus. One can therefore expect that the toroidal version of phase C_{dS} should admit the following minisuperspace action

$$S_{MS}^{(T^3)} = -\frac{1}{24\pi G} \int dt \left(\frac{\dot{V}_3^2}{V_3} - \lambda V_3 \right), \quad (58)$$

where the above potential term is absent.

Using the covariance matrix of spatial volume fluctuations or the effective transfer matrix approach one can again determine the form and parameters of the (discretized) effective action in the toroidal CDT, which is very well described by [25, 26]

$$S_{eff}^{(T^3)} = \frac{1}{\tilde{\Gamma}} \sum_k \left(2 \frac{(N_3(k) - N_3(k+1))^2}{N_3(k) + N_3(k+1)} - \tilde{\lambda} N_3(k) + \tilde{\xi} N_3(k)^\rho \right), \quad (59)$$

where the best fit $\rho \approx -3/2$. Again, as in the spherical CDT, all dimensionless constants appearing in eq. (59), i.e., $\tilde{\Gamma}$, $\tilde{\lambda}$ and $\tilde{\xi}$ depend on the bare couplings of CDT (k_0 and Δ). The kinetic term and the cosmological part of the potential term in equation (59) are consistent with the toroidal minisuperspace action (58).¹³ The additional potential term $\propto V_3^{-3/2}$, where we used the continuum physics notation,

¹² As will be discussed later, the order of the phase transitions can be different.

¹³ As already noted, the CDT effective action and the minisuperspace action agree up to overall sign, see discussion in Conclusions.

does not have a classical counterpart and therefore can be treated as a genuine quantum correction. At the moment it does not have a clear interpretation.

2.2.5 The effective action in other phases

Using the transfer matrix method discussed above one can as well determine the form of the effective action in other phases of CDT. In particular the effective transfer matrix data measured in phase A are well fitted by [24]

$$\langle n|M^{(A)}|m\rangle = \mathcal{N}_0 \exp(\tilde{\lambda}(n+m) - \tilde{\xi}(n^\rho + m^\rho)), \quad \rho \approx 0.5, \quad (60)$$

yielding an effective action without a kinetic term. One can check that indeed when approaching the $A - C_{dS}$ transition from inside the semiclassical phase C_{dS} the measured value of $\tilde{\Gamma} \rightarrow \infty$, causing the kinetic term of the effective actions (40) and (59) disappear at the transition point. Lack of the kinetic term inside phase A can be therefore interpreted as the limit of the effective Newton's constant $G_{eff} \rightarrow \infty$, leading to a causal disconnection of different spatial slices.

The situation is more complicated in phase C_b where the transfer matrix is well parametrized by [24]

$$\begin{aligned} \langle n|M^{(C_b)}|m\rangle = \mathcal{N}_0 & \left[\exp\left(-2 \frac{\left((m-n) - [c_0(n+m-s^b)]_+\right)^2}{\tilde{\Gamma}(n+m-2n_0)}\right) + \right. \\ & \left. + \exp\left(-2 \frac{\left((m-n) + [c_0(n+m-s^b)]_+\right)^2}{\tilde{\Gamma}(n+m-2n_0)}\right) \right] \exp(-V[n+m]), \end{aligned} \quad (61)$$

where: $[...]_+ \equiv \max(\dots, 0)$, and the potential part $V[n+m]$ was not determined precisely. As can be seen from equation (61) the kinetic term of the effective transfer matrix bifurcates for the spatial volume $n+m > s^b$ (the bifurcation point). Hence the other name of the phase C_b , also called the *bifurcation* phase. When approaching the $C_b - C_{dS}$ phase transition from inside the bifurcation phase C_b one observes $s_b \rightarrow \infty$ and $c_0 \rightarrow 0$, resulting in the effective action change at the transition point. Accordingly, in phase C_{dS} one recovers the standard kinetic term of the minisuperspace action. It can be shown that the bifurcation of the kinetic term in phase C_b is related to the appearance of high order vertices in generic triangulations observed in that phase. Such vertices are surrounded by large volume clusters, causing that the volume density is manifestly non-homogeneous, and therefore the minisuperspace description ceases to be valid inside the bifurcation phase C_b .

2.3 Summary of the semiclassical limit

We have shown, that a quantum theory of gravity defined by the four-dimensional Causal Dynamical Triangulations correctly predicts a semiclassical universe with positive cosmological constant, which on large scales is extended and four-dimensional, and whose shape is compatible with a cosmological solution of classical General Relativity. Remarkably, these properties have been derived from first principles in the fully background independent and non-perturbative lattice QFT approach, in which the ground state geometry emerges dynamically from quantum fluctuations. Inside phase C_{dS} the fluctuations of the scale factor are very well described by a simple minisuperspace action. In the thermodynamical limit (when the lattice size $N_4 \rightarrow \infty$) the (relative) amplitude of quantum fluctuations vanishes and one recovers a fully classical trajectory of the scale factor, matching our current understanding of the physics of the very early Universe, at least under the assumption of a spatially homogeneous and isotropic spacetime.

3 Search for a continuum limit

As already mentioned in the introduction, lattice field theories are well suited to study non-perturbative aspects of quantum field theories, such as a (potentially non-perturbatively renormalizable) QFT describing quantum gravity. In the lattice formulation one regularizes a QFT in question by introducing a lattice of size N , where the lattice spacing a plays a role of a UV cutoff $\sim 1/a$. Then, in order to define the continuum limit, one has to remove the cutoff by taking $a \rightarrow 0$ and $N \rightarrow \infty$ in a controlled way, such that the continuum physics quantities of a given QFT remain unchanged. This is related to the renormalization group flow, which describes how the dimensionless bare lattice couplings should be adjusted when approaching the continuum limit. In particular, the QFT is usually characterized by some physical length scale which can be related to a correlation length ξ . While taking the continuum limit $a \rightarrow 0$, the correlation length ξ_a measured in terms of (decreasing) lattice units a must diverge, i.e., $\xi_a \rightarrow \infty$ when $a \rightarrow 0$, such that the physical correlation length $\xi = \xi_a a$ is kept fixed. The diverging correlation length is characteristic for a higher-order phase transition. Therefore the presence of the higher-order transitions in a lattice theory is a *sine qua non* condition of the existence of the continuum limit and the related renormalization group fixed point(s). We thus have a space of (dimensionless) bare coupling constants associated with the lattice theory and we want to locate regions in this space where there are higher-order phase transitions. In this section we will discuss how the order of a phase transition can be measured using numerical MC methods and we will provide evidence that (at least some of) the CDT phase transitions are indeed the higher order transitions. Then

we will try to define the CDT renormalization group flow, following the paths of "constant physics" in the direction of decreasing lattice spacing.

3.1 Phase transitions

Phase transitions can typically be captured by analyzing some macroscopic properties of a given system and tracking their changes when varying coupling constants of a theory in question. The notion of an order of a phase transition was introduced by Ehrenfest, who proposed to characterize phase transitions using derivatives of thermodynamical potentials, such as free energy, measured at the transition point. According to the Ehrenfest classification, if all first $(n - 1)$ derivatives of the free energy are continuous and the n -th order derivative diverges at the transition point then one has the n -th order phase transition. This picture was refined by Landau and Ginzburg who introduced the notion of an order parameter (OP).¹⁴ The order parameter is related to the first-order derivative of the free energy and it captures the symmetry difference between the two different phases. Since then the classification of phase transitions shifted towards distinguishing between two types of phase transitions: first-order, which has a divergent first-order derivative of the thermodynamic potential, and higher-order (also called continuous), where the first-order derivative is continuous but second- or higher-order derivatives diverge. Therefore, in the case of a first-order transition an order parameter is discontinuous at the transition point and one observes a δ -like singularity of susceptibility related to a second-order derivative of a thermodynamical potential. The behaviour is different for a higher-order phase transition, where an order parameter is continuous but it is non-analytic at the transition point. As a consequence the second- or higher-order derivatives diverge in a specific way. Furthermore, in the above classification, there is a relation between the order of a transition and the correlation length. For a first-order transition one typically has finite correlation length, while divergent correlation length signals a continuous phase transition. As will be discussed below, the distinction between orders of phase transitions using lattice methods is non-trivial. This is caused by the fact that in a lattice formulation one deals with a large but finite number of degrees of freedom and thus both the thermodynamical potentials and all their derivatives are finite. Therefore, instead of observing true phase transitions one in fact deals with *pseudo phase transitions* (cross-overs), causing much smoother transition signals. It is only in the thermodynamical limit, i.e., when the lattice size $N \rightarrow \infty$, that one recovers the true phase transitions. It is therefore necessary to analyze finite-size

¹⁴ One should note that in some recent models of solid state physics the Ehrenfest-Landau-Ginzburg characterization can fail, when a phase transition cannot be characterized by a local order parameter, but rather by long-range entanglement, called topological order. Nevertheless in the following we will stick to the proposed classification of phase transitions.

effects and discuss how the lattice results can be interpolated to the infinite volume (lattice size) limit.

3.1.1 Ising model example

As a toy model example let us discuss the Ising model of a ferromagnet with the nearest neighbours interaction on a (d -dimensional) square lattice of size N (denoting the number of vertices where spins are placed), described by a partition function

$$Z(\beta, h) = \sum_{\{s_i\}} \exp \left(\beta \sum_{i \leftrightarrow j} s_i s_j + h \sum_i s_i \right), \quad s_i = \pm 1, \quad (62)$$

where $\{s_i\}$ in the first sum denotes all possible spin configurations. In the model there are two (dimensionless) coupling constants β and h , related respectively to the inverse temperature and the external magnetic field.¹⁵ In the thermodynamical limit, for $d \geq 2$ dimensions and without external field ($h = 0$) one has a second-order (continuous) phase transition between the ordered and the disordered phase occurring at the critical (inverse) temperature β_c .¹⁶ The Ising model with external field can be also used to describe a first-order phase transition between positive and negative magnetization occurring for $\beta > \beta_c$ (low temperature) at $h_c = 0$.

Higher-order transition

Let us start with a second-order phase transition in the absence of the external field ($h = 0$). The macroscopic properties of the system can be traced by magnetization (per spin)

$$m = \frac{1}{N} \sum_i s_i. \quad (63)$$

It plays a role of an order parameter distinguishing between the low temperature (high β) ordered phase, where the system is magnetized ($\langle m \rangle \neq 0$), and the high temperature (low β) disordered phase, where the magnetization vanishes ($\langle m \rangle \approx 0$). In the disordered phase the spins are distributed randomly and one recovers a (spin-inversion) Z_2 symmetry of the Hamiltonian (with $h = 0$), while in the ordered phase the spins prefer to align together and therefore spontaneously break the Z_2 symmetry. Accordingly, the order parameter captures the difference between symmetries of generic spin configurations observed in the two phases.¹⁷ The average magnetization

¹⁵ We used a (non-standard) convention in which h is the inverse temperature \times the external field.

¹⁶ In $d = 2$ dimensions $\beta_c = \frac{1}{2} \ln(1 + \sqrt{2}) \approx 0.44$

¹⁷ Note that formally the Z_2 symmetry is present also in the ordered phase as in any finite temperature there is a non-zero probability of tunnelling between the positive and the negative magnetization which are equally probable. This can be observed for small lattices. Therefore one often uses $|m|$

$$\langle m \rangle = \frac{1}{N} \left\langle \sum_i s_i \right\rangle = \frac{1}{N} \frac{1}{Z} \sum_{\{s_i\}} \sum_i s_i \exp \left(\beta \sum_{i \leftrightarrow j} s_i s_j + h \sum_i s_i \right) = \frac{1}{N} \frac{\partial \ln Z}{\partial h}, \quad (64)$$

is related to a first-order derivative of the free energy $F = -\frac{1}{\beta} \ln Z$.

One can as well compute the (magnetic) susceptibility χ which is the first-order derivative of the (average) magnetization and thus the second-order derivative of the free energy

$$\chi = \frac{\partial \langle m \rangle}{\partial h} = \frac{1}{N} \frac{\partial^2 \ln Z}{\partial h^2}. \quad (65)$$

It follows that

$$\frac{\chi}{N} = \langle m^2 \rangle - \langle m \rangle^2, \quad (66)$$

so the susceptibility χ is proportional to the magnetization variance. The susceptibility

$$\chi = \frac{1}{N} \sum_{ij} (\langle s_i s_j \rangle - \langle s_i \rangle \langle s_j \rangle) = \frac{1}{N} \sum_{ij} G_c^{(2)}(i, j) = \sum_j G_c^{(2)}(0, j) \quad (67)$$

is also related to the (connected) two-point correlation function defined by

$$G_c^{(2)}(i, j) = \frac{\partial^2 \ln Z}{\partial h_i \partial h_j}, \quad (68)$$

where we have introduced a space-dependent external field ($h \rightarrow h_i$). Generically, away from the transition point the correlation function decays exponentially

$$G_c^{(2)}(i, j) \sim e^{-|x_{ij}|/\xi}, \quad (69)$$

where $|x_{ij}|$ is the distance between two lattice points i and j , and ξ is the correlation length, which depends on the parameters of the system, i.e., $\xi = \xi(N, \beta, h)$. Typically the correlation length is of order of a few lattice units a . Interesting physics arises when $\xi \rightarrow \infty$. This is achieved in the thermodynamical limit $N \rightarrow \infty$ by fine-tuning the coupling constant(s) to the critical value(s), i.e., for the Ising model $\beta \rightarrow \beta_c$. In the neighborhood of a continuous phase transition the exponential fall-off in equation (69) vanishes and the correlator starts to behave according to the power law

$$G_c^{(2)}(i, j) \sim \frac{1}{|x_{ij}|^{d-2+\eta}} \quad (70)$$

instead of m as an order parameter, as $\langle |m| \rangle$ is manifestly non-zero in the ordered phase. The tunnelling probability decays exponentially with N thus in practice for large lattices the tunnelling never happens in the MC simulation time, and one can as well use $\langle m \rangle$.

where η is a critical exponent. As a result correlations extend to macroscopic distances $|x_{ij}| \gg a$ and the system starts to be insensitive to the short-distance details of the lattice. Therefore, in the vicinity of the higher-order critical point, one can possibly obtain a continuum limit of a theory microscopically defined on a lattice. As microscopic details of the lattice become unimportant there will be many theories with a different microscopic formulation but the same properties in the continuum limit, such a phenomenon is called *universality* and it is mostly governed by the same symmetries and dimensionality of different systems. The (universal) non-analytic behaviour near a continuous phase transition point is captured by scaling relations. In the thermodynamical limit $N \rightarrow \infty$ one has in the transition region

$$\xi \sim |\beta_c - \beta|^{-\nu}, \quad (71)$$

$$\langle m \rangle \sim |\beta_c - \beta|^\alpha, \quad (72)$$

$$\chi \sim |\beta_c - \beta|^{-\gamma}, \quad (73)$$

where ν , α and γ are critical exponents.¹⁸ For a finite lattice of size N the pseudo-critical point $\beta_c(N)$ is shifted relative to the true critical point $\beta_c = \beta_c(\infty)$. Also the largest length scale available on a finite lattice is of the order of the linear extension of the lattice $L = N^{1/d}$ and thus instead of the infinite correlation length at the phase transition one has $\xi(N) \sim N^{1/d}$. Using equation (71) one obtains

$$|\beta_c - \beta_c(N)|^{-\nu} \sim N^{1/d}, \quad (74)$$

leading to the following finite-size scaling relation of the pseudo-critical point

$$\beta_c(N) = \beta_c - \text{const} \times N^{-\tilde{\nu}}, \quad \tilde{\nu} = \frac{1}{\nu d}. \quad (75)$$

As suggested by equation (73), for fixed lattice volume N one can find a pseudo-critical point $\beta_c(N)$ by observing a peak in susceptibility. The scaling exponent $\tilde{\nu}$ can be then computed numerically by performing a series of MC measurements for larger and larger lattices and fitting the scaling relation (75). For a higher-order (continuous) transition one expects $\tilde{\nu} < 1$, e.g., for the two-dimensional Ising model one has $\tilde{\nu} = 1/2$.

Similarly, using equation (74) one obtains the following finite size scaling relations

$$\langle m \rangle \sim N^{-\tilde{\alpha}}, \quad \tilde{\alpha} = \alpha \tilde{\nu}, \quad (76)$$

$$\chi \sim N^{\tilde{\gamma}}, \quad \tilde{\gamma} = \gamma \tilde{\nu}. \quad (77)$$

The scaling exponents $\tilde{\alpha}$ and $\tilde{\gamma}$ can again be computed numerically by measuring the values of the (average) magnetization and susceptibility at the pseudo-critical

¹⁸ The critical exponent α is usually denoted β but here we used a different notation to distinguish it from the (inverse) temperature. For the two-dimensional Ising model one has $\nu = 1$, $\alpha = 1/8$, $\gamma = 7/4$.

points $\beta_c(N)$ and then fitting equations (76) and (77), respectively. For higher order transitions one expects $\tilde{\alpha}, \tilde{\gamma} < 1$.

First-order transition

The Ising model that we have been investigating also exhibits a phase transition between positive and negative magnetization which can be achieved for $\beta > \beta_c$ (low temperature) through the introduction of an external magnetic field h . By the symmetry it is expected that the transition occurs at $h_c = 0$, where the (average) magnetization $\langle m \rangle$ jumps from positive to negative values. The jump in magnetization means that there is a discontinuity of the first-order derivative of the free energy and thus the transition is first-order. Consequently, one can also expect to observe a δ -like singularity in the magnetic susceptibility χ , which is a first-order derivative of the magnetization and the second-order derivative of the free energy.

Conversely to the higher-order transition case, the correlation length stays finite and there are no long-range collective fluctuations in the system. As a result the rearrangement of spin configurations from positive to negative magnetization is difficult. In the thermodynamical limit $N \rightarrow \infty$ one observes a hysteresis which causes the phase change to occur at points slightly displaced from $h_c = 0$. The hysteresis occurs due to metastable states of positive and negative magnetization coexisting at the critical point. In numerical simulations, the hysteresis is visible only for large enough lattices, as for large N the MC simulation time is usually shorter than the MC autocorrelation time at the transition point, which is large and grows exponentially with (some power of) N . For smaller lattices, where the autocorrelation time is much shorter than the MC simulation time, one can observe back and forth tunnelling between the two metastable states in the transition region ($h \approx 0$). This causes that the transition is smoothed and thermodynamical quantities become continuous and "rounded" for finite N , e.g., instead of the jump in magnetization one observes a tanh-like behaviour of $\langle m \rangle$, similarly instead of δ -like behaviour of susceptibility there is a smooth peak in χ . This shows that in practice the accurate estimation of jumps in the expectation value of an order parameter and singularities in its susceptibility at phase transitions which are only "weakly" first-order is particularly cumbersome and then even the distinction from second-order transitions may be a problem. Therefore again one has to perform a careful finite-size scaling analysis in order to extrapolate from the smooth behaviour of a finite system towards jumps and singularities of $N \rightarrow \infty$.

Typically, in the case of a first-order transition the probability distribution of an order parameter in the transition region can be described by a sum of two shifted Gaussians, centered at values characteristic for the two metastable states coexisting at the transition point. In particular, in the Ising model the behaviour of magnetization m is well approximated by the following probability distribution [27]¹⁹

¹⁹ For the Ising model the double Gaussian approximation can be derived using Landau-Ginzburg theory formulated in terms of free energy. It is not accurate in the region between the two peaks,

$$\begin{aligned}
p(m) &= \mathcal{N} e^{hmN} \left[\exp\left(-\frac{(m - \bar{m})^2}{2\bar{\chi}/N}\right) + \exp\left(-\frac{(m + \bar{m})^2}{2\bar{\chi}/N}\right) \right] \\
&= \tilde{\mathcal{N}} \left[e^{h\bar{m}N} \exp\left(-\frac{(m - \bar{m} - h\bar{\chi})^2}{2\bar{\chi}/N}\right) + e^{-h\bar{m}N} \exp\left(-\frac{(m + \bar{m} - h\bar{\chi})^2}{2\bar{\chi}/N}\right) \right],
\end{aligned} \tag{78}$$

where \mathcal{N} , $\tilde{\mathcal{N}}$ are normalization factors. For $h = 0$ one recovers two equally probable metastable states of magnetization centered at $\pm\bar{m}$ and the amplitude of fluctuations within each state is governed by $\bar{\chi}$ (note that $\bar{\chi}$ is not the total susceptibility but rather a susceptibility within each state).²⁰ The width of the two Gaussians decreases with N and in the limit $N \rightarrow \infty$ one obtains two shifted δ -functions. It is also visible that the non-zero external field h shifts the position of the two Gaussians in the direction of h and the shift is proportional to h . At the same time the relative probability of observing each state changes with h , such that for $h > 0$ the peak at positive m becomes exponentially larger than the peak at negative m , while for $h < 0$ the opposite happens and thus negative magnetization prevails, and the effect is stronger for larger N .

It is a simple task to compute $\langle m \rangle$ and χ using probability distribution (78). One obtains

$$\langle m \rangle = \bar{\chi}h + \bar{m} \tanh(h\bar{m}N), \tag{79}$$

$$\chi = \frac{\partial \langle m \rangle}{\partial h} = \bar{\chi} + \bar{m}^2 N / \cosh(h\bar{m}N). \tag{80}$$

This explains the smoothed tanh-like behaviour of magnetization (instead of a jump) as well as a smooth peak of height proportional to N in susceptibility (instead of a δ -like function) observed for finite N . Away from the critical point, i.e., for $|h| \gg |\bar{m}N|^{-1}$ one recovers the expected "bulk" behaviour

$$\langle m \rangle \approx \bar{\chi}h \pm \bar{m}, \quad \chi \approx \bar{\chi}, \tag{81}$$

whereas in the transition region, i.e., for $|h| \ll |\bar{m}N|^{-1}$, one has

$$\langle m \rangle \approx h\bar{m}^2 N, \quad \chi \approx \bar{m}^2 N. \tag{82}$$

It follows that at the first-order critical point one obtains the following universal finite-size scaling relations²¹

$$\langle m \rangle \sim N, \quad \chi \sim N. \tag{83}$$

since there $p(m)$ reflects interfacial contributions of spin clusters, but (for large enough N) probability density in this region is very small so it contributes only negligible corrections to $\langle m \rangle$ and χ .

²⁰ In other models the positions of states don't have to be symmetric w.r.t. zero and also the widths of the two Gaussians can differ.

²¹ For the Ising model one formally has $\langle m \rangle = 0$ at $h_c = 0$.

Note, that the only scaling which enters the above equations is related to the total volume of the system (lattice size N). This is different than the scaling observed for higher-order transitions, see equations (76) and (77), where one has non-trivial scaling exponents. In the Ising model discussed here, due to the spin-inversion symmetry at $h = 0$, there will be no shift of the pseudo-critical point with N as always $h_c(N) = 0$. Nevertheless, in other models which exhibit first-order transitions one can also expect a finite-size scaling of the pseudo-critical point, similar to equation (75), where again the scaling will be related to the total volume N , i.e., one has a trivial scaling exponent $\tilde{\nu} = 1$, being the only power of N which comes into play for the first-order transition.

3.1.2 CDT phase transitions

As discussed above, phase transitions belonging to the same universality class will show the same type of finite-size scaling properties, which manifest by universal values of scaling exponents and in principle can be used to distinguish between first- and higher-order transitions. The Ising model example shows that a practical distinction between the two types of phase transitions using lattice methods is non-trivial and requires a careful analysis of finite-size effects. In both cases pseudo-critical points can be found by tracking an order parameter \mathcal{O} , used to distinguish the two different phases, and observing a peak in its susceptibility

$$\chi_{\mathcal{O}} \equiv \bar{N}_4 \left(\langle \mathcal{O}^2 \rangle - \langle \mathcal{O} \rangle^2 \right), \quad (84)$$

where \bar{N}_4 denotes the lattice size, i.e., the (constant) target four-volume fixed in the MC simulations of CDT.²² In the MC simulations, for each lattice size N , one typically changes values of one coupling constant (below denoted C , in the case of CDT: $C \equiv k_0$ or Δ , respectively) while keeping other coupling(s) fixed and one can therefore measure the finite-size scaling of the pseudo-critical point $C_c(N)$

$$C_c(\bar{N}_4) = C_c - \text{const} \times \bar{N}_4^{-\tilde{\nu}}, \quad (85)$$

where the critical exponent $\tilde{\nu} = 1$ indicates a first-order transition while $\tilde{\nu} < 1$ a higher order transition. One could look as well at the average value of an order parameter $\langle \mathcal{O} \rangle$ or its susceptibility $\chi_{\mathcal{O}}$ measured at the pseudo-critical points $C_c(N)$ and use finite-size scaling relations

$$\langle \mathcal{O} \rangle \sim \bar{N}_4^{-\tilde{\alpha}}, \quad (86)$$

²² In CDT one often performs MC simulations by fixing $\bar{N}_4 \equiv \bar{N}_4^{(4,1)}$, i.e., the total number of $T^{(4,1)}$ and $T^{(1,4)}$ simplices, instead of true $\bar{N}_4 = \bar{N}_4^{(4,1)} + \bar{N}_4^{(3,2)}$, also including $T^{(3,2)}$ and $T^{(2,3)}$ simplices.

$$\chi_O \sim \bar{N}_4^{\tilde{\gamma}}, \quad (87)$$

where again $-\tilde{\alpha} = 1$ and $\tilde{\gamma} = 1$ point to a first-order transition while other values of the critical exponents indicate a higher-order transition. In practice the relations (86) and (87) are rarely used in CDT as the observed phase transitions are quite "narrow" and the resolution of the numerical data is insufficient to measure the average value of an order parameter at the transition point or the susceptibility peak value with good enough accuracy.

Another possibility of distinguishing between first- and higher-order phase transitions comes from observing two different metastable states present for the first-order transition and absent for the higher-order transition. For example, one can analyze empirical distributions (histograms) of order parameters measured at pseudo-critical points. As explained for the Ising model, the two metastable states cause double peaks in the probability distributions. If a phase transition is "strongly" first-order one can also observe hysteresis in the transition region. However, as CDT results show, one should again very carefully analyze finite-size effects, as it can happen that the hysteresis (or the two peaks separation) shrinks to zero in the $N \rightarrow \infty$ limit. The appearance of double peaks in the histograms is well quantified by the, so-called, Binder cumulant, related to the 4-th moment of the probability distribution²³

$$B_O \equiv \frac{1}{3} \left(1 - \frac{\langle O^4 \rangle}{\langle O^2 \rangle^2} \right). \quad (88)$$

For a first-order transition, where the histograms have two shifted peaks, B_O measured at the critical point will move away from zero when $N \rightarrow \infty$ as the two peaks become more and more apparent (the probability distribution approaches two shifted δ -functions). If instead the transition is higher-order, then the histograms have only one peak and B_O should tend to zero for $N \rightarrow \infty$. Thus a deviation of B_O (measured at the critical point) from zero in the limit $N \rightarrow \infty$ can indicate a first-order transition while a value close to zero suggests a higher-order transition. In Table 1 we summarize the characteristics of both types of phase-transitions which were used in CDT to distinguish between the first- and the higher-order transitions.

Last but not least one should discuss what order parameters have been used in CDT. In the Ising model example the order parameter (the magnetization m) was conjugate to the external field h appearing in the Hamiltonian and playing a role of a coupling constant in the model. Similarly, in CDT one has three coupling constants: k_0 , Δ and k_4 and one can thus use the conjugate quantities, i.e., the global numbers N_0 , $N_4^{(4,1)}$ and $N_4^{(3,2)}$ characterizing a CDT triangulation and appearing in the Regge action. Usually in the MC simulations one fixes the total lattice volume $N_4^{(4,1)}$. Consequently

²³ Note that here, and in general in the CDT phase transitions studies, we use a definition of the Binder cumulant which is shifted (by a $-2/3$ constant) versus the original Binder's definition [28]: $B_O = 1 - \frac{1}{3} \frac{\langle O^4 \rangle}{\langle O^2 \rangle^2}$.

Table 1 Characteristics of the first- and the higher-order phase transitions.

OBSERVABLE	First-order transition	Higher-order transition
Pseudo-critical point scaling according to (85)	$\tilde{\nu} \approx 1$	$\tilde{\nu} < 1$
Susceptibility scaling according to (87)	$\tilde{\gamma} \approx 1$	$\tilde{\gamma} < 1$
Hysteresis in the transition region	YES and remains when $\bar{N}_4 \rightarrow \infty$	NO or disappears when $\bar{N}_4 \rightarrow \infty$
Histograms measured at pseudo-critical points	double peaks peak separation \uparrow with $\bar{N}_4 \rightarrow \infty$	single peak or peak separation \downarrow with $\bar{N}_4 \rightarrow \infty$
Binder cumulant measured at pseudo-critical points	$B_O < 0$ when $\bar{N}_4 \rightarrow \infty$	$B_O \approx 0$ when $\bar{N}_4 \rightarrow \infty$

one has the following order parameters²⁴

$$O_1 = \frac{N_0}{N_4^{(4,1)}} \quad , \quad O_2 = \frac{N_4^{(3,2)}}{N_4^{(4,1)}}. \quad (89)$$

One can as well use more local information, not captured by the "global" order parameters defined above. For example, even though the total lattice volume $N_4^{(4,1)}$ is fixed in the MC simulations, its distribution over spatial slices (the volume profile $N_3(k)$) is not and the generic spatial volume distribution can vary among different phases. Similarly, there is a global relation between N_0 and $N_4^{(4,1)} + N_4^{(3,2)}$, captured by an average coordination number of a vertex²⁵, but the typical coordination numbers of individual vertices can be very much different between generic triangulations observed in different phases. Therefore one can define two more order parameters

$$O_3 = \frac{1}{N_4^{(4,1)}} \sum_k \left(N_3(k) - N_3(k+1) \right)^2 \quad , \quad O_4 = \frac{1}{N_4^{(4,1)}} \operatorname{argmax}_v (c(v)), \quad (90)$$

where v denotes a set of all vertices in a triangulation and $c(v)$ is the coordination number. The behaviour of all four order parameters in various CDT phases is presented in Fig. 8. At a first glance it may seem a little bit surprising that in addition to the "typical" order parameters O_1 and O_2 , which are conjugate to the bare couplings of CDT appearing in the Regge action (3), we have introduced new order parameters O_3 and O_4 , not related to the bare action. We did it for pragmatic reasons, as the new order parameters enable us to study some phase transitions, like the $C_b - C_{dS}$ transition, which are not visible using the "typical" order parameters. Nevertheless one could say that the same happens in the "pure" (meaning without the external field, i.e., for $h = 0$) Ising model, which undergoes a higher-order phase transition at $\beta = \beta_c$. In order to define the expectation value and susceptibility of an order

²⁴ Note that similarly to the Ising model, where one used an intensive magnetization per spin m , in CDT we also normalize by the lattice volume $N_4^{(4,1)}$.

²⁵ The coordination number is defined as a number of 4-simplices sharing a given vertex.

parameter (magnetization) in terms of derivatives of the free energy one has to "enlarge" the Ising model by introducing a new coupling h , related to the external field. Similarly, in the case of CDT one can "enlarge" the model by adding non-trivial couplings to local degrees of freedom, not appearing in the bare Regge action of CDT (3). For example, O_4 has exactly such interpretation as it can be related to a non-trivial measure term (dependent on local order of vertices) introduced in some lattice models of quantum gravity [7]. It turns out that indeed the order parameter O_4 is very well suited to detect the $C_b - C_{dS}$ transition related to the appearance of high-order vertices, characteristic for phase C_b and not present in phase C_{dS} , see Fig. 8.

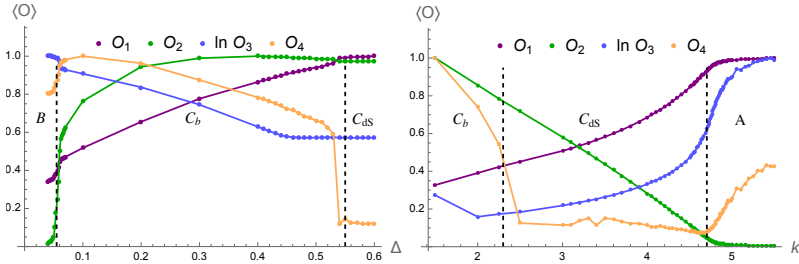


Fig. 8 CDT order parameters, see equations (89) and (90), measured in the toroidal CDT for fixed $k_0 = 1.5$ (left panel) and for fixed $\Delta = 0.4$ (right panel). The order parameters were rescaled to fit into range $[0, 1]$. Phase transitions are indicated by dashed lines.

Using the order parameters $O_1 - O_4$ one can measure phase transition characteristics described above (see Table 1) and thus in principle distinguish between the first- and the higher-order transitions. In practice, the distinction is not always easy as phase transition signals are mixed for most CDT transitions. Therefore, we take a cautious approach, i.e., even in a case where most characteristics point to a higher-order transition but there are some signals of a first-order transition we classify the transition in question as the first-order transition. Using these rules one has the following: in both the spherical and the toroidal CDT, the $A - C_{dS}$ transition was found to be a first-order transition [29, 30], while the $B - C_b$ transition is a higher-order transition [29, 31]. As regards other CDT phase transitions the picture is more complicated. The $C_b - C_{dS}$ transition was found to be a higher-order transition in the spherical CDT [32], but a first-order transition in the toroidal CDT [12]. The $B - C_{dS}$ transition and the $A - B$ transition was so far studied only in the toroidal model, where both transitions were found to be first-order [33]. The above results are summarized in Table 2. The order of the transitions is also depicted in Fig. 2, where blue solid lines denote first-order transitions, while red solid lines are higher-order transitions.

Let us stress that the CDT phase transitions are non-standard from the point of view of ordinary phase transitions, since they involve changes in spacetime geometry and the related effective topology, rather than changes in field configurations on a

Table 2 Summary of CDT phase transitions.

PHASE TRANSITION	Spherical CDT	Toroidal CDT
$A - C_{dS}$	first-order	first-order
$B - C_{dS}$?	first-order
$C_b - C_{dS}$	higher-order	first-order
$B - C_b$	higher-order	higher-order
$A - B$?	first-order

fixed spacetime, like, e.g., in the Ising model. First, let us clarify what we mean by *effective topology*. In order to understand that let us consider spacetime configurations observed in the de Sitter phase C_{dS} in the spherical CDT, i.e., when the fixed spatial topology is S^3 and (due to time-periodic boundary conditions) the total topology of the triangulations is that of $S^1 \times S^3$. By construction, any MC update of a triangulation cannot change the imposed total topology. However, a generic configuration in phase C_{dS} will effectively look like an S^4 -triangulation where the north-pole and the south-pole of the four-sphere are connected by a thin "stalk" of cut-off size, cf. average spatial volume profiles in Fig. 4. The "stalk" is necessary to preserve the imposed total topology of the triangulations, but if only it was allowed by the MC algorithm it would completely disappear, yielding the change of the topology from $S^1 \times S^3$ to S^4 (which we call the effective topology). It is thus visible that not only the effective spacetime dimension but also the effective spacetime topology can be emergent concepts on the quantum level.

Now an interesting pattern emerges linking the order of the CDT phase transitions with the effective topology of spacetimes observed in the adjacent phases. As discussed above, the effective topology of phase C_{dS} in the spherical CDT is that of S^4 . The same effective topology is also observed (both in the spherical and the toroidal CDT) in the bifurcation phase C_b . At the same time the spherical CDT $C_b - C_{dS}$ transition is a higher-order transition. Also the effective topology of phase B is similar and the $B - C_b$ transition is a higher-order transition (both in the spherical and the toroidal case). All other phase transitions observed so far in CDT are first-order transitions and they are related to a change of the effective topology. In the case of toroidal CDT, the $B - C_{dS}$ transition and the $C_b - C_{dS}$ transition involve a change of the effective topology from S^4 (observed in phases B and C_b) to T^4 (in the toroidal version of phase C_{dS}). The effective topology of phase A may be characterized as the topology of a disjoint union of spatial geometries, and thus it is different from the effective topologies encountered in other CDT phases, and again the $A - B$ and the $A - C_{dS}$ transitions are first-order transitions. The above results lead to the following conjecture:

phase transitions which involve a change in effective topology will be first-order transitions.

At the same time all CDT transitions which don't involve the effective topology change are most likely higher-order transitions.

3.2 RG flow in CDT and the perspective continuum limit

Our main interest is to find a higher-order phase transition where one may be able to define a continuum limit of CDT. Since only the phase C_{dS} seems to offer acceptable infrared configurations, it is natural to look for the higher-order transition lines at the border of that phase. From the results reported above, we cannot use the toroidal CDT in such studies, since all such transition lines are first-order.²⁶ Therefore we will focus on the spherical CDT, where one observes that the $C_b - C_{dS}$ transition line is higher-order. According to our conjecture, it is also likely that the spherical $B - C_{dS}$ transition (whose order has not been determined yet) is a higher-order transition, as it separates phases of the same effective topology. It also potentially makes the $C_b - B - C_{dS}$ triple point an interesting candidate for a UV-fixed point. At least it would then be a critical point where three higher-order transition lines meet.

Having located the higher-order phase transition line(s) we now want to understand how to approach the critical point(s) from inside the physically interesting phase C_{dS} . The general idea is quite simple: we would like to adjust the dimensionless bare couplings of CDT in such a way that the RG trajectories in the (k_0, Δ) coupling constant space, i.e., the lines of "constant physics" defined by some renormalized continuum observables, flow in the direction of decreasing lattice spacing a and hopefully lead to the higher-order critical point, implying that the correlation length $\xi_a \rightarrow \infty$ and the lattice spacing $a \rightarrow 0$. Then such a critical point will correspond to a UV fixed point in which one obtains a continuum limit of the CDT lattice theory. The absence of a UV fixed point would be signaled by the fact that there is not any RG flow line ending at a higher-order transition point. In that case one cannot shrink the lattice spacing to zero and obtain a continuum limit. In CDT it is convenient to analyze the RG flow of the bare couplings under the additional assumption that the (average) physical volume of spacetime is fixed and finite along each RG flow trajectory

$$V_4 \propto N_4 a^4 = \text{const.} \quad (91)$$

Accordingly, one has to increase lattice volume N_4 in an appropriate way when the lattice spacing a is decreased, and the thermodynamical limit $N_4 \rightarrow \infty$ will coincide with the continuum limit $a \rightarrow 0$, if it exists.

The key question remains: how to define what constitutes a line of "constant physics"? In the following we will use a definition introduced in [34] (see also [3] for discussion), where "constant physics" relies on two quite natural assumptions, namely that (i) the "shape" of the (average) CDT geometry and (ii) the (relative) amplitude of quantum fluctuations remain constant on each RG flow trajectory. As will be shown below such a definition has important consequences for the renormalized gravita-

²⁶ There is still a chance that the triple points, i.e., the points where the three transition lines meet, see Fig. 2, may potentially be higher-order critical points, as it is quite common to observe a higher-order critical point in the end of a first-order transition line. But this is hard to check numerically.

tional coupling constant if the semiclassical description in terms of the (Euclidean) de Sitter universe and the minisuperspace effective action introduced in Section 2.2 stays valid up to the UV scale.

As discussed in Section 2.2, the (average) CDT geometry inside the semiclassical phase C_{dS} seems to be consistent (at least when the scale factor is considered) with the (Euclidean) de Sitter universe, i.e., a regular four-sphere S^4 . It implies a relation between the measured parameter $\tilde{\omega}$, quantifying the width of the CDT geometry in lattice units, and its continuum counterpart ω , set by a condition that the total four-volume of the sphere equals V_4 , see equation (38),

$$\tilde{\omega} = \omega C_4^{1/4}.$$

There is also a relation between $\tilde{\omega}$, ω and the coupling constants $\tilde{\mu}$, μ appearing in the minisuperspace (39) and the CDT (40) effective actions, respectively, see equation (42),

$$\tilde{\mu} \tilde{\omega}^{8/3} = \mu \omega^{8/3} = \text{const.}$$

Following [34], let us now consider anisotropic space-time scaling scenarios à la Hořava-Lifshitz gravity [10, 35, 36].²⁷ In the cosmological minisuperspace truncation one recovers the continuum semiclassical volume profile (35), as well as the continuum minisuperspace effective action (39), but now ω becomes a free parameter, which quantifies the space-time anisotropy, and consequently the volume profile (35) corresponds to a deformed S^4 geometry, i.e., a four-ellipsoid, compressed or elongated in time direction depending on ω (for $\omega = (\frac{3}{8\pi^2})^{1/4}$ one recovers the symmetric S^4). In such a case also the above relation (42) between ω and μ stays valid, and thus the space-time asymmetry, quantified by ω , is set by the value of (dimensionless) coupling constant μ appearing in the minisuperspace action (39) ($\mu = 9(2\pi^2)^{2/3}$ corresponds to a symmetric case consistent with General Relativity). As a result, though relation (38), different values of the lattice parameter $\tilde{\omega}$ will translate into different values of the continuum parameter ω and thus to a physically different geometry of the quantum universe. Consequently

$$\tilde{\omega}(k_0, \Delta) = \text{const.} \tag{92}$$

is required to keep the (average) continuum geometry fixed and therefore it defines the lines of "constant physics" in the (k_0, Δ) coupling constant space.

In order to define the RG flow one should also require that the relative amplitude of quantum fluctuations stays constant on each line of "constant physics" when approaching the continuum limit, i.e., when the lattice volume N_4 is increased and the lattice spacing a is decreased in accordance with equation (91). The condition

²⁷ One should note that such an approach manifestly breaks the four-dimensional diffeomorphism invariance of the continuum theory by introducing a preferred time-foliation and thus makes the asymmetry between space and time a real physical phenomenon.

$$\frac{\sqrt{\langle \delta V_3^2(t_k) \rangle}}{\langle V_3(t_k) \rangle} = \frac{\sqrt{\langle \delta N_3^2(k) \rangle_{\tilde{N}_4}}}{\langle N_3(k) \rangle_{\tilde{N}_4}} = \text{const.} \quad , \quad t_k = k a \quad (93)$$

means that one investigates the same "real" continuum physics when changing the cutoff scale, and the result does not depend on N_4 nor a . It cannot be achieved for fixed k_0 and Δ , as in that case relative fluctuations vanish when $N_4 \rightarrow \infty$, see equation (25). Accordingly, the RG flow towards a continuum limit requires following a path of "constant physics" (defined by the condition (92)) in the CDT coupling constant space $(k_0(N_4), \Delta(N_4))$ when N_4 (and therefore $a \propto N_4^{-1/4}$) is changed. The amplitude of spatial volume fluctuations is set by the (renormalized) dimensionless gravitational coupling constant $\tilde{\Gamma}$ (cf. the CDT effective action (40)) and it scales as $\delta N_3 \propto \sqrt{\tilde{\Gamma}} N_4^{1/2}$ (see equation (24)). At the same time $N_3 \propto \tilde{\omega}^{-1} N_4^{3/4}$ (see equation (18)). Therefore the condition (93) implies

$$\frac{\tilde{\Gamma} \tilde{\omega}^2}{N_4^{1/2}} = \text{const.} \quad (94)$$

It means that when the lattice volume N_4 is changed one should follow a RG flow trajectory in the direction where the (renormalized) *dimensionless* gravitational coupling constant $\tilde{\Gamma}$ scales as

$$\tilde{\Gamma}(k_0(N_4), \Delta(N_4)) \propto N_4^{1/2}, \quad (95)$$

where we have explicitly included the dependence of $\tilde{\Gamma}$ on k_0 and Δ . As the amplitude of fluctuations scales as $\delta N_3 \propto \sqrt{\tilde{\Gamma}(k_0, \Delta)}$, the above condition compensates the $N_4^{-1/2}$ factor in equation (94), resulting from a different scaling of the fluctuations and the average volume profiles with N_4 . One should note that combining all RG flow conditions, i.e., equations (91), (92) and (95), leads to (cf. equation (44))

$$G \propto \tilde{\Gamma} \tilde{\omega}^2 a^2 \propto \frac{\tilde{\Gamma} \tilde{\omega}^2}{N_4^{1/2}} = \text{const.} \quad (96)$$

Therefore keeping the same continuum physics when approaching a continuum limit translates into keeping the (renormalized) *dimensionful* gravitational constant G fixed, at least if our effective semiclassical description holds up to this limit.

Summarizing, we assume that each RG flow trajectory is defined by a path in the CDT bare dimensionless coupling constants space $(\kappa_0(N_4), \Delta(N_4))$ parametrized by N_4 (the lattice cutoff scale is $\propto N_4^{1/4}$) which fulfills the following conditions

$$\tilde{\omega}(k_0(N_4), \Delta(N_4)) = \text{const.} \quad , \quad \tilde{\Gamma}(k_0(N_4), \Delta(N_4)) \propto N_4^{1/2}. \quad (97)$$

If the path continues to $N_4 \rightarrow \infty$ ($a \rightarrow 0$), which is possible at a higher-order critical point (k_0^*, Δ^*) , then such a point will be a UV fixed point.

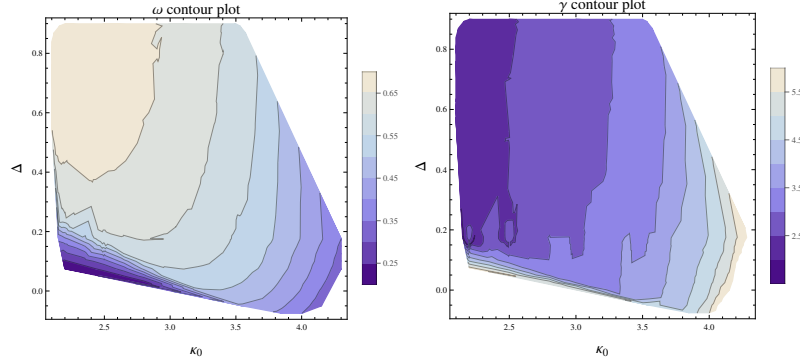


Fig. 9 The "shape" parameter $\tilde{\omega}$ (left panel) and the fluctuations amplitude $\gamma \propto \sqrt{\tilde{\Gamma}}$ (right panel) measured in the spherical CDT for $\tilde{N}_4^{(4,1)} = 40k$. Courtesy of J. Ambjørn and A. Görlich.

In order to check if the conditions (97) can be satisfied one can perform a series of MC simulations in a grid of points (k_0, Δ) to measure the distributions $N_3(k)$ and then compute $\tilde{\omega}(k_0, \Delta)$ and $\tilde{\Gamma}(k_0, \Delta)$. Our analysis assumes that $\tilde{\omega}(k_0, \Delta)$ and $\tilde{\Gamma}(k_0, \Delta)$ do not depend on \tilde{N}_4 which, as discussed in Section 2.2, is indeed the case inside the phase C_{dS} for large enough \tilde{N}_4 . It is therefore enough to carry out measurements for a fixed lattice volume \tilde{N}_4 . The results of such measurements [34] performed for $\tilde{N}_4^{(4,1)} = 40k$ are visualized in Fig. 9, where we show contour plots of $\tilde{\omega}(k_0, \Delta)$ (left panel) and $\sqrt{\tilde{\Gamma}(k_0, \Delta)}$ (right panel) in the (k_0, Δ) -plane. The lines visible on the left plot can be directly interpreted as lines of "constant physics", where $\tilde{\omega}(k_0, \Delta) = \text{const}$. Moving along any such line one can read off from the right plot how $\sqrt{\tilde{\Gamma}(k_0, \Delta)}$ changes and thus in which direction one should follow when N_4 is increased (i.e., the lattice spacing a is decreased). It is seen that the lattice spacing decreases towards the right-bottom corner of the plots, i.e., towards the interesting region of the CDT phase diagram, where higher-order transition lines meet. It is also seen that most of the RG flow trajectories, which are deep inside the C_{dS} phase, go parallel to the $C_b - C_{dS}$ phase transition line but then turn away and go parallel to the $A - C_{dS}$ phase transition line. Therefore such RG flow lines do not lead to any UV fixed point. However, there are potentially some lines of "constant physics" (very close to the $C_b - C_{dS}$ phase transition line) which may lead to a common critical point, cf. Fig. 10.

3.3 Summary of the search for a continuum limit

Examples of simple lattice models, such as the Ising model, show that determining the order of a phase transition may be a difficult task and one has to carefully analyze

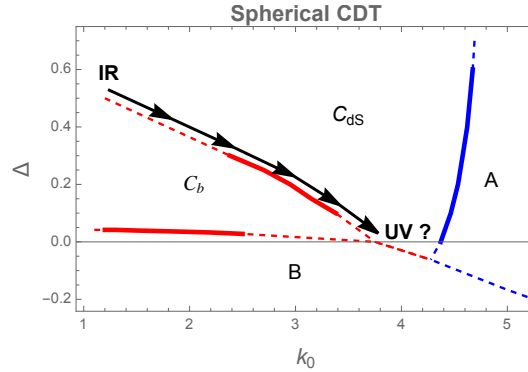


Fig. 10 Putative CDT renormalization group flow line(s) leading from the IR to the (perspective) UV fixed point.

finite-size effects. In the case of CDT additional complication comes from the fact that the CDT phase transitions are not typical phase transitions studied in "standard" lattice QFTs, defined on the fixed spacetime, but they rather involve changes in spacetime geometry or even spacetime (effective) topology. Nevertheless, using numerical MC simulations, one can study properties of the CDT phase transitions and in principle distinguish between the first- and the higher-order transitions. The results of the CDT phase transition studies performed so far lead to the conclusion that only in the case of the spherical CDT one can observe the higher-order phase transition lines (the $C_b - C_{ds}$ phase transition and potentially the $B - C_{ds}$ phase transition) bordering the physically interesting phase C_{ds} , inside which one observes the IR semiclassical universe. In that case one can also define the RG flow trajectories, related to keeping the physical "shape" of the universe and (relative) amplitude of quantum fluctuations fixed and leading in the direction of decreasing lattice spacing. Combining RG flow conditions with an assumption that the physical four-volume of the universe is kept fixed leads to a condition that the *dimensionful* gravitational coupling constant G is kept fixed on each RG flow line up to the UV scale, see equation (96). One should note that this result is not compatible with the standard functional renormalization group approach to asymptotic safety, where the *dimensionless* gravitational coupling stays non-zero but the dimensionful $G \rightarrow 0$ as the UV cutoff is removed. Thus comparing results of both approaches is difficult and requires further studies. Nevertheless, despite most of the RG flow trajectories in CDT do not end up in a common UV fixed point, there are some trajectories which potentially lead to a continuum limit, as schematically outlined in Fig. 10. The results are not conclusive as the precision of the MC measurements discussed above was not good enough to make sure that the RG flow really goes to the genuine UV fixed point(s).

4 Conclusions

Causal Dynamical Triangulations is based on lattice QFT techniques applied to the quantization of gravity and uses only a few additional assumptions about the topology of spacetime. Lattice QFTs turned out to be very successful in addressing many non-perturbative problems in other areas of physics, e.g., regarding Quantum Chromodynamics (QCD) beyond perturbation regime. QCD is an ordinary QFT in flat spacetime and the regular hyper-cubic lattice used represents a simple discretization of the flat spacetime. However, if the field theory is gravity, spacetime itself becomes non-trivial and dynamical. Therefore CDT generalizes the conventional lattice QFT to the case of fluctuating geometries, approximated by lattices constructed from a few types of simplices with fixed edge lengths. Using Regge prescription of how to compute spacetime curvature for a simplicial manifold one can express Einstein-Hilbert action in terms of dimensionless lattice variables. The Regge action is defined in terms of geometric invariants, such as lengths and angles, and does not use spacetime coordinates, thus making CDT diffeomorphism-invariant. CDT is also manifestly background independent as all possible (lattice regularized) spacetime geometries enter the quantum-gravitational path integral. The key non-trivial assumption of CDT is that the quantum spacetime is globally hyperbolic and therefore can be foliated into spatial slices of constant cosmological time, which all have the same fixed topology. Although the distinguished notion of time in CDT looks superficially similar to the time-foliation in Horava-Lifshitz gravity [35], its status is different because CDT does not possess any residual diffeomorphism invariance, which therefore cannot be broken either. The role of time in CDT was partly clarified in a study in three dimensions, where it was verified explicitly that key results of CDT quantum gravity continue to hold in a version of the theory which does not possess a preferred time foliation [37]. This provides strong evidence that the notion of time that is naturally available in standard CDT is simply a convenient foliation choice (a la gauge fixing) and that its presence does not affect the results of the theory in an unwanted way. The CDT time-foliation enables one to precisely define what is meant by a Wick rotation from the Lorentzian to the Euclidean spacetime signature and thus one can use the (Euclidean) model to investigate properties of the quantum-gravitational path integral using numerical Monte-Carlo methods.

One of the greatest achievements of CDT is that it correctly predicts the IR limit of quantum gravity, consistent with classical Einstein's field equations. The semiclassical limit is obtained in the, so-called, de Sitter phase C_{dS} , where one observes the emergent four-dimensional average geometry with superimposed quantum fluctuations. What is more, fluctuations of the global "shape" of the universe, quantified by the time evolution of the scale factor, are very well described by a simple minisuperspace effective action. One should note that despite the fact that the observed semiclassical solution for the scale factor is consistent with a homogeneous and isotropic universe, the above mentioned symmetries are not put in by hand in CDT (as it is done in minisuperspace models), but emerge dynamically, as also does the

effective spacetime dimension four. It is quite remarkable that despite the fact that the geometries entering the gravitational path integral are very non-classical, after performing a suitable average over configurations the scale factor gets consistent with a homogeneous and isotropic spacetime. However, since the scale factor is just one mode of the metric, in order to verify that the observed semiclassical ground state geometry is really homogeneous and isotropic one should use some other observables quantifying the "average geometry". This is still an open issue, but some progress has been recently made in this direction, see [38, 13, 39]. Another non-trivial result is that the CDT effective action agrees with the standard Euclidean minisuperspace action only up to overall sign (cf. equations (39) and (40), where both $\Gamma, \bar{\Gamma} > 0$). The standard Euclidean minisuperspace action is unbounded from below due to negative sign of the kinetic term. The sign of the action does not matter for a classical trajectory but in the path integral formalism the unbounded action causes the path integral to be completely dominated by arbitrarily large fluctuations of the conformal mode, making the quantum theory ill-defined. A cure to the conformal mode problem can possibly come from a specific contour of integration for the conformal factor as Hartle and Hawking proposed in their minisuperspace truncation of the gravitational path integral [40]. In CDT the problem is cured in a natural way without resorting to the Hartle-Hawking "trick", as one automatically obtains the inverted sign of the kinetic term, exactly consistent with the Hartle-Hawking proposal. This simply comes from a subtle interplay between the purely geometric degrees of freedom (entering the bare Regge action of CDT) and the entropic factor (counting the number of states with the same value of the bare action), which seems to stabilize the underlying quantum theory.

Another good feature of the four-dimensional CDT is that it has a rich phase structure, where (in the case of spherical CDT) some of the phase transitions bordering the physically interesting semiclassical phase C_{dS} seem to be higher-order transitions. As a result one may hope to test the asymptotic safety scenario, where the UV fixed point of quantum gravity should appear as a higher-order critical point. Accordingly, one can try to define the RG flow of the CDT bare coupling constants towards the fixed point. If the RG flow leads to a higher-order critical point in such a way that the transition point could be associated with a gravitational UV fixed point one would obtain a non-perturbative description of a theory which can be viewed as the quantum theory of gravity defined at arbitrarily short distances or, alternatively, at arbitrarily large energy scales. The results reported in Section 3.2 are not conclusive as the resolution of numerical data is not good enough to make sure if (at least some) of the RG flow lines lead to a higher-order critical point. One should also note that the above results were obtained [34] before the $C_b - C_{dS}$ phase transition was discovered [24], and therefore at that moment the results were missing our current understanding of the CDT phase structure. It would be then worth to repeat the RG flow measurements using current computer resources and improved algorithms of the MC simulations which would enable to study much larger systems thus reducing finite-size effects and increasing accuracy of the numerical results. Having said this, let us comment about a possible scenario that the continuum limit cannot be found.

First of all it can mean that our definition of what is considered to be a line of "constant physics" (here defined as a constant "shape" of the semiclassical CDT universe) is wrong and one should use some other notions of "constant physics", which can be well motivated by nonclassical features of quantum geometry found on Planckian scales. This is indeed possible as the CDT approach seems to be non-compatible with the standard renormalization group techniques used in asymptotic safety. It leads again to the problem of defining good observables quantifying such features. But even in the most pessimistic scenario, where the new observables wouldn't help, CDT could still be considered as an effective QFT of gravity, valid up to some finite energy scale of order of the Planck's scale.

References

- [1] S. Weinberg. "Ultraviolet Divergences in Quantum Theories of Gravitation". In: *General Relativity: An Einstein Centenary Survey*. 1980, pp. 790–831.
- [2] F. Saueressig. "Causal Dynamical Triangulations and the Renormalization Group". In: *Handbook of Quantum Gravity*. 2023.
- [3] J. Ambjørn. "(Causal) Dynamical Triangulations: a Regularization of Quantum Gravity". In: *Handbook of Quantum Gravity*. 2023. arXiv: 2209.06555 [hep-lat].
- [4] J. Ambjørn et al. "Nonperturbative Quantum Gravity". In: *Phys. Rept.* 519 (2012), pp. 127–210. doi: 10.1016/j.physrep.2012.03.007. arXiv: 1203.3591 [hep-th].
- [5] R. Loll. "Quantum Gravity from Causal Dynamical Triangulations: A Review". In: *Class. Quant. Grav.* 37.1 (2020), p. 013002. doi: 10.1088/1361-6382/ab57c7. arXiv: 1905.08669 [hep-th].
- [6] J. Ambjørn et al. "CDT Quantum Toroidal Spacetimes: An Overview". In: *Universe* 7.4 (2021), p. 79. doi: 10.3390/universe7040079. arXiv: 2103.15610 [gr-qc].
- [7] J. Laiho. "Review of Euclidean Dynamical Triangulations". In: *Handbook of Quantum Gravity*. 2023.
- [8] T. Regge. "General Relativity Without Coordinates". In: *Nuovo Cim.* 19 (1961), pp. 558–571. doi: 10.1007/BF02733251.
- [9] J. Ambjørn, J. Jurkiewicz, and R. Loll. "Dynamically triangulating Lorentzian quantum gravity". In: *Nucl. Phys. B* 610 (2001), pp. 347–382. doi: 10.1016/S0550-3213(01)00297-8. arXiv: hep-th/0105267.
- [10] J. Ambjørn et al. "CDT meets Horava-Lifshitz gravity". In: *Phys. Lett. B* 690 (2010), pp. 413–419. doi: 10.1016/j.physletb.2010.05.054. arXiv: 1002.3298 [hep-th].
- [11] J. Ambjørn et al. "Signature Change of the Metric in CDT Quantum Gravity?" In: *JHEP* 08 (2015), p. 033. doi: 10.1007/JHEP08(2015)033. arXiv: 1503.08580 [hep-th].

- [12] J. Ambjørn et al. “The phase structure of Causal Dynamical Triangulations with toroidal spatial topology”. In: *JHEP* 06 (2018), p. 111. doi: 10.1007/JHEP06(2018)111. arXiv: 1802.10434 [hep-th].
- [13] G. Clemente and M. D’Elia. “Spectral Observables and Gauge Field Couplings in Causal Dynamical Triangulations”. In: *Handbook of Quantum Gravity*. 2023.
- [14] M. Reitz et al. *Generalised spectral dimensions in non-perturbative quantum gravity*. 2022. arXiv: 2207.05117 [gr-qc].
- [15] M. Craioveanu, M. Puta, and T. Rassias. *Old and New Aspects in Spectral Geometry*. 2001. doi: 10.1007/978-94-017-2475-3.
- [16] J. Ambjørn, J. Jurkiewicz, and R. Loll. “Spectral dimension of the universe”. In: *Phys. Rev. Lett.* 95 (2005), p. 171301. doi: 10.1103/PhysRevLett.95.171301. arXiv: hep-th/0505113.
- [17] O. Lauscher and M. Reuter. “Ultraviolet fixed point and generalized flow equation of quantum gravity”. In: *Phys. Rev. D* 65 (2001), p. 025013. doi: 10.1103/PhysRevD.65.025013.
- [18] D. Benedetti. “Fractal Properties of Quantum Spacetime”. In: *Phys. Rev. Lett.* 102 (2009), p. 111303. doi: 10.1103/PhysRevLett.102.111303.
- [19] P. Horava. “Spectral Dimension of the Universe in Quantum Gravity at a Lifshitz Point”. In: *Phys. Rev. Lett.* 102 (2009), p. 161301. doi: 10.1103/PhysRevLett.102.161301.
- [20] L. Modesto. “Fractal spacetime from the area spectrum”. In: *Classical and Quantum Gravity* 26 (Nov. 2009), p. 242002. doi: 10.1088/0264-9381/26/24/242002.
- [21] J. Ambjørn et al. “Nonperturbative quantum de Sitter universe”. In: *Phys. Rev. D* 78 (2008), p. 063544. doi: 10.1103/PhysRevD.78.063544.
- [22] J. Ambjørn et al. “The semiclassical limit of causal dynamical triangulations”. In: *Nucl. Phys. B* 849.1 (2011), pp. 144–165. doi: https://doi.org/10.1016/j.nuclphysb.2011.03.019.
- [23] J. Ambjørn et al. “The Transfer matrix in four-dimensional CDT”. In: *JHEP* 09 (2012), p. 017. doi: 10.1007/JHEP09(2012)017. arXiv: 1205.3791 [hep-th].
- [24] J. Ambjørn et al. “The effective action in 4-dim CDT. The transfer matrix approach”. In: *JHEP* 06 (2014), p. 034. doi: 10.1007/JHEP06(2014)034. arXiv: 1403.5940 [hep-th].
- [25] J. Ambjørn et al. “Impact of topology in causal dynamical triangulations quantum gravity”. In: *Phys. Rev. D* 94.4 (2016), p. 044010. doi: 10.1103/PhysRevD.94.044010. arXiv: 1604.08786 [hep-th].
- [26] J. Ambjørn et al. “Four-dimensional CDT with toroidal topology”. In: *Nucl. Phys. B* 922 (2017), pp. 226–246. doi: 10.1016/j.nuclphysb.2017.06.026. arXiv: 1705.07653 [hep-th].
- [27] K. Binder and D. P. Landau. “Finite-size scaling at first-order phase transitions”. In: *Phys. Rev. B* 30.3 (1984), p. 1477. doi: 10.1103/PhysRevB.30.1477.

- [28] K. Binder. “Critical Properties from Monte Carlo Coarse Graining and Renormalization”. In: *Phys. Rev. Lett.* 47 (1981), pp. 693–696. DOI: 10.1103/PhysRevLett.47.693.
- [29] J. Ambjørn et al. “Second- and first-order phase transitions in causal dynamical triangulations”. In: *Phys. Rev. D* 85 (2012), p. 124044. DOI: 10.1103/PhysRevD.85.124044.
- [30] J. Ambjørn et al. “Critical phenomena in causal dynamical triangulations”. In: *Classical and Quantum Gravity* 36.22 (2019), p. 224001. DOI: 10.1088/1361-6382/ab4184.
- [31] J. Ambjørn et al. “The higher-order phase transition in toroidal CDT”. In: *JHEP* 05 (2020), p. 030. DOI: 10.1007/JHEP05(2020)030. arXiv: 2002.01051 [hep-th].
- [32] D. Coumbe, J. Gizbert-Studnicki, and J. Jurkiewicz. “Exploring the new phase transition of CDT”. In: *JHEP* 02 (2016), p. 144. DOI: 10.1007/JHEP02(2016)144. arXiv: 1510.08672 [hep-th].
- [33] J. Ambjørn et al. “Topology induced first-order phase transitions in lattice quantum gravity”. In: *JHEP* 04 (2022), p. 103. DOI: 10.1007/JHEP04(2022)103.
- [34] J. Ambjørn et al. “Renormalization Group Flow in CDT”. In: *Class. Quant. Grav.* 31 (2014), p. 165003. DOI: 10.1088/0264-9381/31/16/165003. arXiv: 1405.4585 [hep-th].
- [35] P. Horava. “Quantum gravity at a Lifshitz point”. In: *Phys. Rev. D* 79 (2009), p. 084008. DOI: 10.1103/PhysRevD.79.084008.
- [36] Y. Sato. “CDT and Horava-Lifshitz QG in Two Dimensions”. In: *Handbook of Quantum Gravity*. 2023. arXiv: 2212.03446 [hep-th].
- [37] S. Jordan and R. Loll. “Causal Dynamical Triangulations without preferred foliation”. In: *Phys. Lett. B* 724.1 (2013), pp. 155–159. DOI: <https://doi.org/10.1016/j.physletb.2013.06.007>.
- [38] R. Loll. “Observables and curvature in CDT”. In: *Handbook of Quantum Gravity*. 2023.
- [39] A. Görlich. “Scalar Fields in Four-Dimensional CDT”. In: *Handbook of Quantum Gravity*. 2023.
- [40] J. Hartle and S. Hawking. “Wave function of the Universe”. In: *Phys. Rev. D* 28 (1983), pp. 2960–2975. DOI: 10.1103/PhysRevD.28.2960.